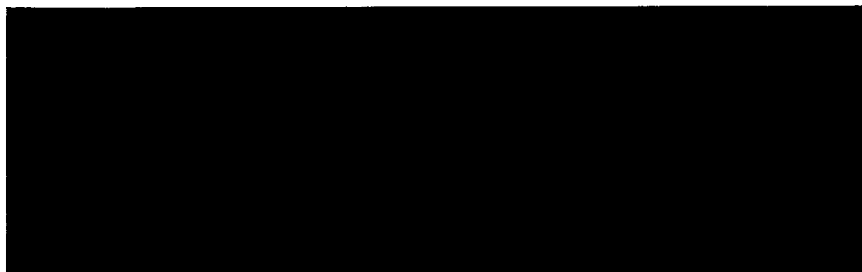




NATIONAL TELECOMMUNICATIONS AND INFORMATION ADMINISTRATION

**Institute for Telecommunication Sciences
Boulder, Colorado 80303**



This document presents project information to an other-agency sponsor.
Additional copies are not available, and this is not a referenceable document.



**Propagation Modeling for IVHS Applications
in the Roadway Environment**

BY

Christopher L. Holloway and Nicholas DeMinco

Propagation Modeling for IVHS Applications in the Roadway Environment

by

Christopher L. Holloway and Nicholas DeMinco

Institute for Telecommunication Sciences
National Telecommunications and Information Administration
U. S. Department of Commerce

July 1994

ABSTRACT

It is expected that the Intelligent Vehicle Highway Systems (IVHS) of the future will involve communication between vehicles and the roadside. In designing these communication systems it is imperative that one has a sound and detailed understanding of radio wave propagation in both short-distance roadside and complicated urban environments. ITS currently has many propagation models for all types of environments including urban environments. In this report the present capabilities of these models are discussed, and the needed improvements to these models are presented that will allow analyzing more complex roadway and urban environments. ITS has approached this problem by examining the radio propagation phenomenon in the roadway environment over the range of distances and at frequencies that will have the potential to meet the needs of IVHS systems. The requirements of the individual functions of IVHS systems were taken into consideration in addition to what portions of the radio frequency spectrum will be available. Also taken into consideration were what systems were available, what manufacturers were planning, and what is being implemented in the FHWA operational tests. The actual evaluation of individual IVHS system performance for IVHS systems and specific FHWA Operational Tests will be performed under additional tasks to be determined after modifications have been made to the propagation models under Phase 2 of the "Propagation Modeling in the Roadway Environment" task.

1 .0 INTRODUCTION

The IVHS systems will probably be implemented using short, radio communication links ranging from meters to hundreds or even thousands of meters. Collision avoidance radars will also work over similar short distances. Radio has not been applied to such functions before, and as a result, radio wave propagation on short paths in the roadway environment has had little attention. This type of environment would most likely contain severe multipath and its effect on different modulation methods would have to be determined. Sufficient knowledge of radio-wave propagation in such an environment is not readily available. Prediction of the behavior of such IVHS systems is difficult at best without this knowledge. This knowledge is necessary for planning, architectural evaluation, system performance prediction, system design and testing, standards development, and standards conformance testing. It is necessary that this knowledge be developed early in the IVHS program. This would allow system performance evaluation of IVHS systems at proposed frequencies.

Characterizing radio wave propagation for various environments has been the object of much attention, especially recently [1]-[5], and includes the work at ITS [6] - [15]. The main difficulty with the bulk of this work is that only line-of-sight (LOS) and limited diffraction propagation channels have been modeled. Only very recently have models of complex out-of-sight (OOS) propagation been investigated such as propagation down side streets and over roof tops [2], [5], [16] and [17]. One problem with these current LOS and OOS models is that simple assumptions about the reflected surfaces and diffraction geometries are made. For example, both the ground and the building walls are assumed to be a perfectly conducting smooth surfaces, but a large class of IVHS problems do not resemble this scenario (see section 4: Tasks # 3,5 and 7). Real surfaces have a finite conductivity and as a result behave much differently.

The purpose of this report is to illustrate the present capabilities of ITS's propagation models and then discuss the needed improvements to the model that would allow the IVHS propagation channels to be analyzed. This report is organized as follows: after the introduction the second section discusses radio wave propagation concepts. In this section, issues pertinent to propagation in both the general roadway and an urban canyon environment are introduced. The present capabilities of ITS's propagation models are discussed in section three, and the prediction of these models compared to experimental results are illustrated. In section four, the improvements needed for the existing models to allow the realistic IVHS channel to be analyzed are introduced and described in detail. Section 5 contains a discussion of frequencies being proposed for use by IVHS systems as a result of what frequencies in the radio spectrum will be available, what manufacturers are proposing for use, what frequencies and systems are proposed for the FHWA Operational Tests, and what makes sense from a propagation point of view.

2. WAVE PROPAGATION CONCEPTS

In this section basic concepts of radio wave propagation will be introduced. In all of the wave interaction concepts discussed here it is assumed that the interaction is taking place in the far field of the source and receptor antennas. The far field of an antenna with effective antenna diameter "D" is governed by the following:

$$Far\ Field > \frac{2 D^2}{\lambda} \quad (1)$$

2.1 FREE SPACE PROPAGATION

If a point source radiates power P_t in all directions, then the power density in the far field at a distance 'r' is given by:

$$S_t = \frac{P_t}{4 \pi r^2} \quad (2)$$

If the transmitting antenna has a directional gain G_t , then the power density at a distance 'r' is now given by:

$$S_t = \frac{G_t P_t}{4 \pi r^2} \quad (3)$$

The power received at an antenna at a distance 'r' with an effective antenna area of A_r is given by:

$$P_r = A_r S_t \quad (4)$$

The gain and the effective antenna area are governed by the well known relationship:

$$A_r = \frac{G_t \lambda^2}{4 \pi} \quad (5)$$

Therefore, the received power for an antenna of gain ' G_r ' at a distance ' r ' away is given by the following:

$$\begin{aligned}
 P_r &= P_t G_t G_r \left(\frac{\lambda}{4 \pi r} \right)^2 \\
 &= P_t G_t G_r \left(\frac{c}{4 \pi f r} \right)^2
 \end{aligned}
 \tag{6}$$

This equation is usually expressed in dB, and is given by:

$$P_r = P_t + G_t + G_r - L_{fs} \quad (dB) \tag{7}$$

where P_r and P_t are the received and transmitted powers respectively in dB, and G_r and G_t are the receiver and transmitter antenna gain respectively in dB. L_{fs} is the free space loss in dB and is given by the following:

$$L_{fs} = 32.45 + 20 \log(f) + 20 \log(r) \quad (dB) \tag{8}$$

where f is the frequency of the radio wave in GHz and r is the distance between the transmitter and receiver in meters.

Equation (7) can be used to calculate the received power for a transmitter and receiver located in free space. This is not the situation for IVHS propagation channels. In the IVHS environment there is at least a conducting ground to deal with and in many situations the wave may have to propagate through a very complicated environment. For example, the energy may have to propagate: through precipitation, through an atmosphere with oxygen and water vapor, through buildings, around corners, down side streets, into and around wooded areas, and over rough terrain. In this type of environment the received signal cannot be expressed by the simple equation given in (7). The remaining part of this section discusses the different types of radio wave interactions that need to be considered for both urban canyon models and general radio-wave propagation models in the roadway environment.

2.2 ATTENUATION DUE TO PRECIPITATION

For radio link systems, precipitation attenuation may be significant depending on the radio frequency and the rate of precipitation. For general IVHS propagation models it is important to have the capability to take account of this added loss if necessary. The attenuation due to precipitation can be taken into account by subtracting the additional loss term 'L_p' (the loss due to precipitation) from equation (7).

Values for 'L_p' have been measured for different precipitation rates and for different radio wave frequencies [18]-[20]. Figures (1)-(4) illustrate the dependance of 'L_p' on precipitation rate and frequencies.

2.3 ATTENUATION DUE TO WATER VAPOR AND OXYGEN ABSORPTION

Attenuation due to clear-air absorption by oxygen and water vapor can have a profound effect on communication systems above approximately 4 GHz. This attenuation can range from a small fraction of a dB/km at 4 GHz up to about 15 dB/km at 100 GHz. This could be important for IVHS applications above 4 GHz. The phase and amplitude response of an electromagnetic wave interacting with the atmospheric medium can be determined by calculating the complex refractive index of the medium. The complex refractive index n of the atmosphere can be used to compute the phase and amplitude of a plane electromagnetic wave propagating a distance d at frequency f from reference [14] as:

$$E(d) = E^o \exp \left(-j 2 \pi \frac{f}{c} d n \right) \quad (9)$$

where E^o is the initial wave amplitude, c is the speed of light in a vacuum, and $j = \sqrt{-1}$. The attenuation L_{ca} (dB) due to clear-air absorption is given by:

$$L_{ca} (dB) = 20 \log \left(\frac{E^o}{E(d)} \right) \quad (10)$$

This loss is also subtracted from equation (7).

2.4 INTERACTIONS WITH PLANAR SURFACES

When radio waves propagate down urban canyons or the short-range roadway environment, they will inevitably be incident onto buildings and onto the ground. Depending upon the nature of these surfaces the reflected wave will behave in different ways. In this section the interaction of radio waves with both smooth and rough surfaces are investigated.

2.4.1 REFLECTION FROM SMOOTH PERFECTLY CONDUCTING SURFACES

If the dimensions of an object are large compared to a wave length, then the object can be treated as a smooth surface. Waves incident onto a smooth surface will be reflected in the specular direction, that is the angle of reflection equals the angle of incidence. When an electric field (E^i) is incident onto a smooth perfectly conducting surface, the boundary condition of Maxwell's Equations indicate that the total tangential field (E^T), that is the incident plus the scattered field (E^s), must be zero:

$$E_{tang}^T = E^i + E^s = 0 \quad (11)$$

This implies that:

$$E^s = - E^i \quad (12)$$

The scattered field can be written in terms of a quantity known as the reflection coefficient (Γ), which is defined as the following:

$$\Gamma = \frac{E^s}{E^i} \quad (13)$$

With this definition, the scattered field is expressed as:

$$E^s = \Gamma E^i \quad (14)$$

Γ is usually written as a complex number which has a magnitude and phase:

$$\Gamma = |\Gamma| e^{j\phi} \quad (15)$$

From equation (12), it is seen that the reflection coefficient for a smooth conducting surface is:

$$\Gamma = e^{j\pi} \quad (16)$$

2.4.2 REFLECTION FROM SMOOTH INTERFACES

If the surface is not a perfect conductor, then the amount of energy that gets reflected in the specular direction is related to the composition of the material and the polarization of the incident wave. It can be shown that the reflection coefficient of an E-field perpendicular (E-polarization) to the plane of incidence is given by:

$$\Gamma_E = \frac{\sin \psi - (\epsilon_r - i 60 \sigma \lambda - \cos^2 \psi)^{1/2}}{\sin \psi + (\epsilon_r - i 60 \sigma \lambda - \cos^2 \psi)^{1/2}} \quad (17)$$

The reflection coefficient of an E-field parallel (H-polarization) to the plane of incidence is given by:

$$\Gamma_H = \frac{(\epsilon_r - i 60 \sigma \lambda) \sin \psi - (\epsilon_r - i 60 \sigma \lambda - \cos^2 \psi)^{1/2}}{(\epsilon_r - i 60 \sigma \lambda) \sin \psi + (\epsilon_r - i 60 \sigma \lambda - \cos^2 \psi)^{1/2}} \quad (18)$$

Some of the reflecting surfaces encountered in IVHS channels will be composed of concrete. Common examples of this are buildings and road surfaces. Figure (5) illustrates the behavior of the reflection coefficient for two polarizations for a infinitely thick slab of concrete at 100 MHz (see [21]). The results shown in this figure were calculated assuming that for dry concrete $\epsilon_r = 6.57$ and $\sigma = 1.96 \cdot 10^{-3}$ (from [22]).

2.4.3 REFLECTIONS FROM ROUGH SURFACES

There are three different scenarios that are encountered with reflections from rough surfaces. The limits of these are governed by the ratio of the dimension of the rough surface to the wavelength of the radio wave, and are discussed below.

2.4.3.1 ROUGHNESS DIMENSION VERY SMALL COMPARED TO LAMBDA

When the roughness dimensions of the surface are very small compared to a wavelength the surface can be treated as a smooth surface. For this particular case, the reflection coefficient is given in equations (16)-(18).

2.4.3.2 ROUGHNESS DIMENSION SMALL COMPARED TO LAMBDA

When the roughness dimensions are small compared to a wavelength and are on the order $\lambda/2$, the rough surfaces can be analyzed with effective boundary condition [23]-[29]. The actual rough surface or interface is replaced by a smooth surface (see Figure (6)) and an effective boundary condition is applied to the smooth surface. The effective boundary condition takes into account the roughness effects.

The effective boundary condition for a perfectly conducting rough surface is treated in [23]-[29]. For this problem it is assumed that all the energy is reflected in the specular direction. Therefore, the magnitude of the reflection coefficient is one. Incident energy is temporarily stored in the roughness profile, causing the phase of the reflected energy to be different than 180 degrees (as for a smooth perfectly conducting surface). The phase of this reflection coefficient is a function of the dimensions of the roughness profile as well as the incident angle. Figure (7) shows the variation of the phase of the reflection coefficient for a rectangular rough profile (see [27] and [28]).

The effective boundary condition for a highly conducting rough interface is treated in [27] and [29]. For this problem it is assumed that some fraction of energy penetrates the rough interface and the remaining energy is reflected in the specular direction. The phase of the reflection coefficient is a function of the roughness profile, the angle of incidence and the conductivity of the surface. Figure (8) shows results for a highly conductive interface (see [27] and [29]).

2.4.3.3 ROUGH DIMENSION LARGE COMPARED TO LAMBDA

When the fields are incident onto a rough surface and the horizontal dimensions of that surface are small compared to a wavelength, then the fields inside the rough troughs cannot develop into higher order propagation modes, hence the energy is reflected in the specular direction. On the other hand, when the dimensions of the roughness profile are large compared to a wavelength, an incident field

can cause higher order modes to propagate. This results in the energy being carried away in directions other than the specular direction. The effect of this is that for a rough perfect conductor, the magnitude of the specular reflection coefficient is no longer one.

This may be explained by referring to Figure (9). A plane wave is incident onto the surface shown in this figure. The phase difference between two rays of the field is:

$$\beta \Delta l = \frac{2 \pi}{\lambda} (2 h \sin \psi) \quad (19)$$

If " $\beta \Delta l$ " is small, the surface can be approximated as smooth. However, if " $\beta \Delta l = \pi$ ", no energy is reflected in the specular direction. For this scenario, the energy is reflected into non-specular directions. Figures (10) and (11) illustrate how the magnitude of the specular reflection coefficient varies as a function of surface dimensions.

There are a number of theoretical approaches that have been taken to analyze electromagnetic (and the mathematically similar acoustic) field problems in the vicinity of rough surfaces. Historically the first approach was probably that of Rayleigh, which was later refined and extended by many works (good accounts of this work may be found in the books [31] and [32]; see also the papers [33]-[38]). For good accounts of periodic rough surfaces see [32], [39] and [40].

2.5 DIFFRACTION FROM OBJECTS

Radio waves propagating down streets will encounter buildings, doors, windows, automobiles and other obstacles with corners. Geometric optics alone can not accurately take into account the electromagnetic field interaction with these corners. For example, assume that a field is incident onto the corner shown in Figure (12). The space in this figure is divided into three regions. The fields in region I consist of the incident field, the reflected field, and fields due to the corner effects (the diffracted field). Region II is referred to as the Reflected Ray Shadow Boundary (RSB). The fields in this region consist of the incident field and the fields due to the corner effects (the diffracted fields). Region III is referred to as the Incident Ray Shadow Boundary (ISB). The fields in this region consist of the diffracted fields only.

If geometric optics is used on this problem, then one would conclude that Region I consists of only incident and reflected fields and Region II consists of only incident fields. Geometric optics says that Region III is null of fields. The Uniform Theory of Diffraction (UTD) [41] and [42] must be used to accurately model the effects of the corners, and then combined with the geometric optics field to model the total radio-wave propagation in the roadway environment.

The diffraction fields are expressed in the following form:

$$E^d = E^i D \frac{e^{-jk s}}{\sqrt{s}} \quad (20)$$

where E^i is the incident field at the diffraction point, s is the distance from the diffraction point to the observation point, k is the wavenumber, and D is the dyadic diffraction coefficient. D is a function of the incident angle, the observation angle, the wave number (k), the distance to the observation point (s), the geometry of the edge, and the material makeup of the edge.

McNamara et al. [42] has expressions for D for perfectly conducting wedges and corners for both two-dimensional and three-dimensional cases. References [43] and [44] give two different expressions for D for an impedance wedge or corners. The first is a rigorous solution of the impedance wedge (see [43]). While the second is based on a heuristic solution (see [44]). Bergljung [2] made a comparison of these two expressions, and the results are reproduced in Figure (13) and (14). These comparisons show that depending on the location of the source with respect to the building corner, the difference between the two expressions can be significant.

Another consideration is building materials. This is so since corners of buildings may behave more like an impedance corner as opposed to a perfectly conducting corner depending on the building materials utilized. We have made comparisons for the diffracted field at a corner of a building assuming both a perfectly conducting corner (McNamara expression [42] for D) and an impedance wedge (Maliuzhinets rigorous expression [43] for D and Luebbers heuristic expression [44] for D), the results are also shown in Figure (13) and (14). From these figures one can see that correctly representing the corners of a building, either as a perfectly conducting corner or as an impedance corner, is important to accurately predicting diffraction around buildings.

Until now we have discussed single diffraction, that is diffraction of an isolated corner or edge. If structures are composed of multiple edges or corners, such as narrow buildings or narrow streets, then coupling between the corners will take place. This type of diffraction is referred to as multiple or higher-order diffraction and is in general a lesser effect than standard single diffraction. However, it plays a bigger role when the separation between the corners is small, and it should then be taken into account. For a detailed account of multiple diffraction see [45] and [46].

3. EXISTING ITS MODELS

In this section we will describe the current radio-wave propagation models that have been developed at ITS. Current ITS models take into account reflecting smooth surfaces that have finite conductivity and permittivity. ITS models also take into account the terrain contours and atmospheric refraction between the transmitter and the receiver and perform diffraction loss computations for the propagation path. ITS has developed several models covering the frequency ranges: from 100 kHz

to 2 MHz, 2 MHz to 30 MHz, 30 MHz to 20 GHz, and 20 GHz to 1000 GHz. Each of these frequency bands are covered by one or more of the specific models to be described in this section.

3.1 General Radio-wave Propagation Models at ITS

ITS has a large number of propagation models for use in analyzing radio communication systems. Some are specialized and others are more general, but all require good engineering judgement on which is the better model to use for a particular analysis. The models described in this section can be used for analysis and prediction of IVHS system performance for medium to long range distances without modification, and short distance LOS radio-wave propagation after certain modifications to account for near-field coupling.

3.1.1 Models for 100kHz to 30MHz

For the frequency bands of 100 kHz to 2 MHz and 2 MHz to 30 MHz both the ground wave and the sky wave must be taken into consideration. Both the sky-wave and the ground-wave model have the capability to interface many different antenna models.

There are two different sky-wave propagation models, one for use above 2 MHz (ITS's IONCAP HF model) and one below 2 MHz (ITS's MF sky-wave model). The sky wave can not only contribute to the desired signal, but in addition it can generate undesirable interference to the desired signal. The desired signal in many cases is the ground-wave signal. IONCAP calculates a myriad of HF sky-wave propagation parameters to enable a complete system analysis to be performed. Typical parameters calculated include: median values of MUF, FOT, LUF, field strength, reliability, antenna gain, noise power, system loss, and signal-to-noise ratio. IONCAP contains the latest CCIR-approved atmospheric noise coefficients, improved manmade noise calculations, and more realistic specifications/predictions for the global variations of the f-region critical frequencies. ITS's MF sky-wave model predicts sky-wave propagation parameters using empirical ionospheric reflection coefficients for an undisturbed ionosphere.

The ground-wave signal can be determined using ITS's Ground Wave Automated Performance Analysis (GWAPA). The ground-wave model computes propagation loss, electric field strength, received power, noise, received signal-to-noise power ratio, and antenna factors over lossy Earth. The smooth-Earth and irregular-Earth (terrain dependent) propagation loss prediction methods can be used over either homogeneous or mixed paths. The main computer program GWAPA combines

three propagation loss prediction methods for both smooth and irregular Earth, a system interface algorithm, a reliability algorithm, and an antenna algorithm into one user-friendly analysis tool. The propagation loss prediction methods, system interface algorithm, and noise prediction algorithm are valid from 10 kHz to 30 MHz.

The ground wave includes the direct line-of-sight space wave, the ground reflected wave, and the surface wave that diffracts around the curved Earth. The following five computation techniques are

used in GWAPA: flat-Earth attenuation function, flat Earth attenuation function with curvature correction, the residue series calculation, geometric optics, and numerical integration of the full-wave theory. The appropriate technique is selected according to the relative geometry of the transmitter and receiver antenna heights and the Earth. Diffraction is accounted for where necessary in the last four of these models. The first model, the flat-Earth attenuation function is used for line-of-sight propagation.

The smooth-Earth method is mathematically and numerically accurate for the ground-wave predictions for frequencies from 10 kHz to 100 MHz, but above 30 MHz the irregularities of the atmosphere make statistical methods more appropriate. Irregularities in the terrain have more of an effect at higher frequencies, so an irregular terrain model is more appropriate when terrain irregularities become appreciable in size with respect to a wavelength.

The smooth-Earth model is valid for all combinations of antenna heights, frequency, and dielectric constants by virtue of the computation techniques contained within its structure. It should be used only out to the maximum ranges considered useful for ground-wave propagation at each frequency, since the sky wave would become significant from that distance to points beyond.

The irregular-Earth, mixed path method uses an integral equation to compute the propagation loss of a vertically polarized electromagnetic wave over irregular terrain that is covered with forests, buildings, or snow. The terrain cover is modeled as a slab of user-specified thickness, length, conductivity, and dielectric constant. Antenna heights of the transmitter and receiver antennas without a slab are taken into account within the program using the same height-gain functions as the smooth-Earth model. When a slab is included, a special height-gain function is used for the antennas within or above the slab. The integral equation approach in this model is a point-to-point prediction method valid for frequencies between 10 kHz and 30 MHz. At higher frequencies, other techniques must be used to take into account the large variability of the ground wave in time and space.

3.1.2 Models for 20 MHz to 20 GHz

The ITS irregular terrain model is a computer method for predicting long-term median radio transmission loss over irregular terrain and is valid over a frequency range of 20 MHz to 20 GHz. The method is based on well-established propagation theory and has been tested against a large number of propagation measurements. Predictions have been tested against data for wide ranges of frequency, antenna height and distance, and for all types of terrain from very smooth plains to extremely rugged mountains. This method can be used with either detailed terrain profiles for actual paths or with profiles that are representative of median terrain characteristics for a given area.

The program requires the input parameters: frequency, antenna heights, and either an estimate of terrain irregularity or the detailed terrain profile. The program computes median reference values of attenuation relative to the transmission loss in free space as a function of distance. The reference attenuation is a certain median attenuation relative to free space. This median is determined from a variety of times and paths when the atmosphere is in a quiet state, well mixed and conforming to a standard atmospheric model.

The calculated reference is based on two-ray geometric optics theory for radio line-of-sight paths with an extrapolated value of diffraction attenuation. The reference value for transhorizon paths is the lesser of either diffraction attenuation or forward scatter attenuation.

Radio propagation in the terrestrial environment at VHF, UHF, and SHF can be very difficult to predict in the physical world, because received signal levels do vary in what appears to be a random fashion. The received signal power varies in time because of changing atmospheric conditions and in space because of changes in terrain. This model is statistical and tries to describe this variability in both the median value of received signal level and the magnitude of the expected deviations from the median value.

3.1.3 Models for 1 GHz to 1000 GHz

The ITS models for this frequency range are the EHF Telecommunication System Engineering Model (ETSEM) for 20 GHz to 100 GHz and the Millimeter Wave Propagation Model (MPM) for 1 GHz to 1000 GHz. The ETSEM model is a terrestrial model for engineering links and the MPM model is a specialized model for computing attenuation due to atmospheric effects. A model that is more general and flexible than either of these two is the Analysis of Microwave Operational Scenarios (AMOS) model for frequencies of 1 to 100 GHz.

The ETSEM model is a line-of-sight model that takes into account Fresnel zone clearances and antenna heights. The program predicts cumulative distribution of propagation losses and converts this to cumulative distribution of received signal level. A climatological data base is used from which the appropriate parameters are interpolated using the midpoint of the path under study. The computations include clear air absorption attenuation due to oxygen and water vapor and attenuation due to rain.

The MPM model is also a line-of-sight model like ETSEM but contains a more rigorous treatment of the clear air absorption attenuation due oxygen and water vapor and the attenuation due to precipitation. The attenuation and propagation delay effects are predicted from meteorological data sets containing pressure, temperature, humidity, suspended particle concentration, and rain rate. Atmospheric propagation limitations have a critical effect on the development of millimeter wave applications. Adverse weather causes reduced radio signals due to rain, wet snow, suspended particles, and water vapor.

The AMOS model provides an integrated procedure for modeling propagation effects on telecommunication links of various scenario types and for predicting system performance. The scenario types include earth to satellite, ground to aircraft, aircraft to satellite, and terrestrial. It is not limited to terrestrial scenarios. The analyses are valid at frequencies between 1 and 100 GHz. The results obtained include rain, clear air, and multipath attenuation using algorithms similar to those in ETSEM and MPM. Received signal levels and link margin calculations are also performed. Terrain profiles are used for terrestrial links to calculate attenuation due to diffraction and troposcatter.

3.2 The ITS Urban Canyon Model

ITS first developed an urban canyon model in 1988 (see Violette et al. [6] and Allen et al. [7]) where a modified ray tracing technique called image space was used to calculate propagation down a city street lined with buildings. This model calculates only line-of-sight (LOS) propagation, and propagation down cross streets (OOS) is not considered.

The building walls in this model are not treated as perfect conductors, but rather as surfaces with reflection coefficients with uniformly distributed magnitude and phase, ranging from 0 to 1 and 0 to 2π respectively. Set values for the reflection coefficient can also be specified if needed. The ground is analyzed as a perfect, smooth conductor with a reflection coefficient of -1. In this model, side streets can be included as regions where no reflections occur. This model does not have the capability of propagating down side streets. The effects of cross streets (or side streets) is approximated by assuming that when a ray encounters a side street, there is no reflection and the ray is lost. This model has since been expanded (now called PCSACM) to account for diffraction from the corners of buildings that are located on cross streets [15]. This latest urban canyon model still only calculates LOS propagation, no cross street or OOS propagation is possible. This model (PCSACM) has been used to estimate line-of-sight (LOS) propagation for an urban canyon illustrated in Figure (15). Figures (16) through (29) (from [15]) show the calculation of the signal strengths for various scenarios, such as, increasing numbers of wall and street reflections, with and without cross streets.

Cross street effects are handled by using diffraction at the four edges of the building at the cross street. The receiver (Rx) is placed at a height of 1.8 m over the ground at points 5m from the near wall. The transmitter (Tx) is placed at a height of 10 m and at a distance of 5 m from the reference wall (see Figure (15)). The beamwidths for both the Rx and Tx antenna are 180 degrees, and are set at an elevation and azimuthal angle of 0 degrees. The frequency used is 1.92 GHz, the transmitted signal power is 0 dBm and the antenna gains are 0 dBi.

Figures (16) through (22) show an example of the area coverage for a urban canyon with no cross streets for line-of-sight (LOS) propagation. Figure (16) considers only free space loss, Figure (17) considers free space loss and one street reflection. Figures (18) through (22) are the same as Figure (17) with an increasing number of wall reflections.

Figures (23) through (29) provide similar information as shown in Figures (16) through (22) except that one cross street has been added. The effects of the cross street are incorporated into the model by taking into account diffraction from the four building corners. Only the free space loss components for the diffracted fields are included, no street or wall reflected components of the diffracted rays are used. The effects of the diffracted fields (or the cross street) can be seen by comparing Figures (16) and (23), Figure (17) and (24), Figures (18) and (25), and so on. The most recent measurements that ITS has for propagation through urban canyons date back to 1983 (see [15] and [47]). These measurements were taken in Denver, Colorado and can be compared to the output of PCSACM (ITS's propagation model). The reflection coefficient for the street and wall were not known, but were set to values which resulted in the best match between the measured and modeled data. The values chosen for the reflection loss for the street and walls were 1 dB and 6 dB, respectively.

For the comparison, a frequency of 9.6 GHz is used and Rx is located at a height of 1.8 m at a distance of 5 m from the wall and is located at a down range position ranging from 50 m to 950 m. Tx is located at a height of 2.15 m at a point 5 m from the wall. The beamwidth of the Tx and Rx antenna are 10.0 degrees and 4.8 degrees, respectively, with respective gains of 25 dBi and 31 dBi. The width of the main street was measured to be 24 m. The distance to the first cross street from the Tx was measured to be 76 m. The width of this cross street was 24 m. Figure (30) shows a comparison of the predicted and measured signal levels as a function of the separation distance between the Tx and Rx. Figures (23) through (30) in Allen [7] show more comparisons between the model and measured signal levels. All these comparisons show fairly good correlation between measured and predicted signal levels for line-of-light (LOS) propagation.

4. IMPROVEMENTS TO ITS PROPAGATION MODELS

The current ITS propagation models described in Section 3.1 can be used for analysis and prediction of IVHS system performance for medium to long range distances without modification, and short distance LOS radio-wave propagation after certain modifications to account for near-field coupling. Improvements need to be made to the current urban canyon model (PCSACM) described in Section 3.2 in order to better predict the signal levels for LOS propagation paths as well as to accurately predict the signal levels for OOS (out-of-sight) propagation paths. Modifications also need to be made to this model to account for near-field coupling. All models should be verified by a carefully planned measurement effort to compare measurements to predictions for similar geometries.

In this section the improvements that are needed to develop the short-range and urban canyon propagation models for IVHS analysis and performance prediction are discussed. These improvements are listed as TASKS which can be performed independently of the other tasks. The intent is to enable investigation of the appropriate tasks that will allow analysis and performance prediction of all types of IVHS systems and subsystems at all different frequencies. Many frequency bands (ranging from AM broadcast band to millimeter wave frequencies and all frequencies in between these limits) have been proposed for all different applications of IVHS functions including: toll collection, vehicle location and identification, traffic information dissemination, collision avoidance, etc.

LIST OF TASKS

TASKS 1: MODELING OUT-OF-SIGHT PROPAGATION

Phase I: Cross streets propagation

The number one improvement that needs to be incorporated in the PCSACM propagation model is propagation down cross streets. The goal here will be to predict the signal level of a receiver placed at location B (see Figure (31)) when the transmitter is located at A. Recent work (see [2], [5], [16] and [17]) investigated propagation down these side streets, and as one might expect, it was found that if the receiver is located close to the intersection, the reflected rays into the side street become the dominant contribution to the signal levels. On the other hand, as the receiver is moved away from the intersection, the diffracted fields from the corners of the building become the dominant contribution to the signal levels. Figures (32) through (34) illustrate the different contributions from the reflected and diffracted fields to the total signal levels.

The coupling of energy into these side streets will require both reflected rays into the side streets as well as diffracted rays from the corner of the building at the main and side street intersection. In this effort, we will modify PCSACM to take into account the propagation down side streets by incorporating both the reflected and diffracted fields.

Phase II: Propagation down multiple side streets

In this task, we will incorporate the ability to predict the multiple side street OOS propagation. That is, to be able to predict the signal level of a receiver located at either point C, D or E with a transmitter located at point A (see Figure (31)). It is believed that the majority of the signal strengths are from the diffracted fields around the corners of the buildings at the various intersections. Therefore, in this effort none of the multiple reflections off the walls will be included. We will include ground reflections of the diffracted fields in the model.

Phase III: Impedance edge and corner diffraction

Depending upon the building materials used, the corners of the building will not appear as perfectly conducting corners, but more like impedance corners. In section 2, we compared the results of the diffracted fields for both a 90 degree perfectly conducting corner, and a 90 degree impedance corner. These comparisons (see Figures (13) and (14)) illustrate that as much as 40 dB difference in the diffracted fields exist for the two cases. This indicates that large errors in the estimated diffracted fields can be achieved if the wrong type of edge or corner condition is used.

In this effort, we will incorporate the option of diffraction from an impedance corner into the PCSACM model.

Phase IV: Diffracted fields from comers to street to receiver

In the current propagation model the diffraction effects are handled in the following manner. The field at the receiver due to diffraction are obtained by only considering a wave from the transmitter hitting the comers of a building and diffracting straight to the receiver. It does not consider a wave diffracting from the comers which then strikes the street and then hits the receiver. The amplitude of this diffracted field is approximately the same as the diffracted fields from the comer hitting the receiver directly. The difference will be found in the phase. This is similar to the effect of the LOS propagation plus reflection from the ground, that is, the diifference in the phase of the two rays causes an interference pattern in the total received signal. Therefore, if we consider both the direct diffracted fields and the reflected diffracted fields one would see an interference pattern in the total diffracted fields depending on the antenna heights and the radio frequency. We have investigated this effect, and the results are illustrated in Figures (35) through (40). In these figures, the total diffracted field (the direct diffracted field plus the ground reflections) is plotted as a function of the receiver distance, measured from the comer of the building for various frequencies and antenna height. Also shown on these figures is the LOS diffraction. One can see that depending upon the frequency and antenna height the total diffracted fields can differ from the LOS diffracted field.

The contribution of the street reflected diffracted fields to the total signal levels may help explain the differences in the predicted to measured signal levels obtained by Yim et al. [17]. His results are reproduced in Figures (32) through (34). In the model presented by Yim et al. [17], prediction of the signal levels down a side street were calculated using the reflections from walls and only the LOS diffracted fields. For large distances down the side street the majority of the signal level is from only the total diffracted fields. The comparison in Figure (32) shows that the predicted signal levels match reasonably well with measurements. However, we see the predicted results appear to have a different slope than the measured data at large distances down the side street (see Figures (33) and (34)). We showed that by considering both the LOS diffracted field and the reflected diffracted field the slope of the signal levels change over that of just considering the LOS diffracted fields, see Figures (35) through (40). Not considering the total diffracted fields could very well explain the difference between the results presented by Yim et al. [17], see Figures (33) and (34).

In this effort we will further investigate the importance of the total diffracted fields (the LOS diffraction and the reflected diiacted field), and if it is found to be important it will be incorporated into the current model.

Phase V: Multiple diffractions from closely spaced comers and objects

In 2.4 it was shown that if comers of buildings are spaced close together, then a second-order diffraction known as “multiple diffraction” will result. This type of diffraction is in general a lesser effect than standard single diffraction. However, it plays a bigger role when the separation between the corners is small, and it should then be taken into account. Multiple diffraction may be more important when predictions down narrow side streets are needed. In this effort will analyze the importance of multiple diffractions and then incorporate this type of diffraction in to the PCSACM model.

TASK 2: MEASUREMENTS OF OUT-OF-SIGHT PROPAGATION

In this task we will undertake a measurement campaign to measure signal levels for out-of-sight (OOS) propagation in different urban canyon scenarios. The measurements can then be used to validate the models developed in TASK 1.

TASK 3: PROPAGATION OVER ROUGH STREETS

All of the propagation models assume that the street is a smooth perfectly conducting plane. In most IVHS applications this assumption is not valid. Propagation of radio waves down urban canyons will occur when the streets are congested with automobiles. If we refer to Figure (41) we see the road surface no longer appears as a smooth surface, but rather as a rough surface. Given the automobile dimensions and the radio wave frequencies to be used for IVHS the roughness dimensions of this rough surface are large compared to a wavelength. In section 2.3.1.2 it was shown that a wave reflecting in the specular direction from a rough surface which has dimensions that are large compared to a wave length, has a reflection coefficient less than one and a phase not equal to 180 degrees. It was also shown that if the dimensions of the rough surface are just right then very little of the energy is reflected in the specular direction, but is reflected in the nonspecular direction.

In Figures (42) through (45), we show results of a signal level at a receiver for a LOS ray and a reflection off the ground, assuming that the phase of the reflection coefficient from the ground is taken from Figure (7). It should be noted that the phase of the reflection coefficient given in Figure (7) is for the situation where the roughness dimensions are small compared to a wavelength, and these do not correlate to the realistic roughness dimensions for roadway propagation. But, using these results gives an indication of how the roughness effects might alter the signal levels. From Figures (42) through (45) we see that the roughness effects not only shift the null of the signal level, but also cause the null and maximum to be less pronounced.

In this task, we will develop a set of curves for the magnitude and phase of the reflection coefficient for typical or realistic roughness dimensions that would be encountered in an IVHS setting. These reflection coefficients for a non-smooth street could then be incorporated into the existing propagation model.

Figure (41) represents automobiles on a street, if these automobiles are in motion with velocity "v", then the rough surface is moving at the velocity "v" of the automobiles. The second phase of this task will be to study the Doppler effects of signal scattering from a rough moving street.

TASK 4: OPTIMAL ANTENNA HEIGHT

We have done a very quick study (see Figure (42) through (45)), and have shown that fading of the total signal levels due to the ground reflection can be minimized, depending upon frequency and antenna height. In this task we will investigate what might be the optimal transmitter and receiver height for an IVHS system.

TASK 5: PROPAGATION DOWN ROADS IN THICKLY FORESTED AREAS

The IVHS system may need to work in areas where the roadway is lined with thick forest. In order to accurately model propagation in this type of environment it is important to accurately characterize the reflection coefficient from the forest boundary. This characterization could be accomplished either by measuring reflection coefficients or by theoretically modelling the reflection from a free space/tree interface.

Individuals in the past have theoretically modeled this problem [48]-[52]. In this work, it is assumed that " Γ " (the reflection coefficient) could be determined in the same manner that it is determined when two regions are homogeneous and isotropic, that is the reflection coefficient was calculated by:

$$\Gamma = \frac{\eta_{eff} - \eta_o}{\eta_{eff} + \eta_o} \quad (21)$$

where the " η_{eff} " is the effective material properties of a wave propagating into the forest. However, evidence suggests (see Holloway [29] and [53]) that this approach does not accurately predict the reflection coefficient. Holloway [53] has shown that a correction term is needed in equation (21), that takes into account the higher-order modes that are present at the air-tree interface.

In the IVHS environment there may also be a need to propagate through foliage. This is a very complex problem, however, Yacoub [54] has introduced empirical formulas for propagation through foliage. The attenuation for a vertically polarized wave is given by:

$$L = 1637 \sigma + \frac{\log \left(1 + \frac{f}{10} \right) \cdot e^{-\frac{90}{f}}}{2.99} \quad \frac{dB}{m} \quad (22)$$

and for a horizontally polarized wave the attenuation is given by:

$$L = 1637 \sigma + \frac{\log \left(1 + \frac{f}{200} \right) \cdot e^{-\frac{210}{f}}}{2.34} \quad \frac{dB}{m} \quad (23)$$

where " σ " is the conductivity (S/m) and "f" is the frequency in MHz. Some values for " σ " are given in Table (1).

In this task, these expression can be incorporated into the propagation model. We are proposing to experimentally determine the reflection coefficients from a forest/air interface. Another part of this effort is to theoretically investigate the error that occurs in calculating the reflection coefficient by not considering the correction as mentioned above.

TASK 6: PROPAGATION THROUGH TUNNELS AND BRIDGES

In many urban settings, automobiles drive on bridges composed of complex metal structures as well as through different types of tunnels. The metal structure of the bridges and the material content of the tunnels results in very complicated propagation channels for IVHS which may in turn compromise the efficiency of the IVHS system. Attenuation of the signal levels in these types of environments can be sever. Figures (46) and (47) (page 87 from Yacoub [54] and page 112 from Jakes [55]) illustrate the effects of frequency and antenna spacing on the attenuation of the signal propagating through a tunnel. The best way to approach this type of propagation environment is not entirely clear, so part of this task will be to investigate different techniques to determine the best way to model propagation through tunnels and bridges.

TASK 7: PROPAGATION THROUGH BUILDINGS

Depending upon the building material used, the straight line propagation path through the buildings (point A to C, A to D, or A to E, see Figure(31)), may be a significant contribution to the total signal. We may find that the propagation through the building can be the same order of magnitude as the diffracted fields down two to three city blocks. In earlier work, Alexander [56] and Seidel et al. [57] performed measurements of signal propagation through the indoors of buildings. They found that the free space loss did not vary as the typical $1/r^2$, but varied as $1/r^n$. Where n could be a number ranging from 1.2 to 6.5, depending on the type of building material (see Table (2)). An experimental effort similar to that done by Alexander [56] and Seidel [57] for the indoor channel will need to be performed on various urban canyon settings, in order to accurately characterize the $1/r^n$ propagation loss for different types of buildings. In this effort the straight line propagation through the building model for the multiple side street scenario will be incorporated into PCSACM.

TASK 8: COMPENSATION FOR NEAR-FIELD AND CLOSE-IN DISTANCES

The models described in Section 3 of this report will need some compensation to allow for near-field coupling in situations where the distances between the transmitter and receiver of an IVHS communication system are so close that a far-field analysis is an invalid approach for performance prediction. The electromagnetic waves arriving at a receiver from a transmitter at such short distances is not a true plane-electromagnetic wave and the antennas are not effectively characterized by their far-field gains. At these close-in distances the field strength or received power from the transmitter does not depend on the far-field gains of the transmitter and receiver antennas. A near-field analysis approach is the correct way to analyze IVHS systems operating under these conditions. One analysis approach would examine the near field of both the specific transmitter and receiver antennas separately and combine the results to compute either signal field intensity or power at the receiver. Another approach would be to perform a near-field coupling calculation using the specific electrical characteristics and physical geometry of configuration under study. In this effort near-field coupling techniques will be incorporated into the models described in Section 3.

5. DISCUSSION

IVHS systems will probably be implemented using short radio communication links ranging from meters to hundreds or even thousands of meters depending on the particular application. There will be a need for collision radars working over similar short distances.

In this report we have introduced some of the propagation issues that need to be considered in the IVHS roadway environment. The current capabilities of ITS's propagation models that can be applied to analysis and prediction of IVHS systems in the roadway environment have also been described. The improvements to the existing ITS models have been described that are needed to accurately predict propagation for IVHS systems in the roadway environment. The intent is to enable investigation of the appropriate tasks that will allow analysis and performance prediction of all types of IVHS systems and subsystems at all different frequencies.

Modification of existing IVHS models and the subsequent measurements that will allow verification of these revised models will be necessary for the planning, architectural evaluation, system performance prediction, system design and testing, standards development, and standards conformance testing.

The type of function the IVHS system must perform would suggest potential bands of the frequency spectrum where the nature of radio wave propagation physics would permit that function to be performed. That area of the frequency spectrum would also have to be available or reassigned for use. Based on the physics of the different IVHS functions, certain areas of the radio frequency spectrum would be suitable for collision avoidance and other areas would be more appropriate for position location, dissemination of information to vehicles, communication between vehicles and the roadside, emergency beacon location, toll collection, etc.

ITS has determined what existing propagation models could be applied to characterize the propagation phenomena in the roadway environment at these frequencies. In addition, ITS has proposed what additional research and/or measurements that need to be performed to develop other propagation algorithms for system performance prediction of IVHS systems. This propagation model development and measurements would be performed in phase II of this task.

Many frequency bands (ranging from AM broadcast band to millimeter wave frequencies and all frequencies in between these limits) have been proposed for all different applications of IVHS functions including: toll collection, vehicle location and identification, traffic information dissemination, collision avoidance, etc. The following discussion will describe the IVHS user services and functions proposed for use. In addition, the frequencies at which manufacturers are planning to build IVHS systems for the Federal Highway Administration operational tests have also been taken into consideration.

The information on frequencies that are being planned for use in IVHS systems is based on the activities of the IVHS Communications Committee. A frequency requirements matrix was generated from essentially four activities of this committee. Those activities were: the Transportation research board (TRB) in San Francisco, the Communications Spectrum Task Force, the "A" team from the Communications Committee, and the Group of Experts Meeting (March 16-17, 1994). Many of the Federal Highway Administration's Operational Tests are testing systems at the frequencies in this matrix. The matrix will not be repeated here, but the information taken from it will be used to indicate what frequency ranges are important to IVHS systems and will need the appropriate propagation models for analysis and performance prediction.

The 902-928, 2450, and 5800 MHz bands are likely candidates for many IVHS applications. The 902-928 MHz band has the advantage of having the cheapest equipment implementation, but it also has the greatest number of users in it, so it will probably be too crowded in the near future with ISM, Government radars, and Part 15 devices. Manufacturers prefer this band due to the low cost of equipment in this band compared to other bands. The 2450 MHz band has moderate cost equipment, but it too is also very crowded with microwave ovens near the center of the band. The Government is giving up part of the band at the low end. The 5800 MHz band has the highest equipment cost, but there is very little ISM or Part 15 usage yet. There is a possibility to use either the 5.1 GHz band (now allocated for the Microwave Landing System (MLS)) or the 4.6 GHz band to be given up by the Federal Government. The Canadians use the 4.6 GHz band heavily for point-to-point communications, which could make this band unsuitable for use as a North American Standard.

The applications and functions in the IVHS Communications Committee matrix will be listed by frequency in the following separate subsections. These are bands that the activities of the IVHS Communications Committee decided would be useful for IVHS applications. The performance of these IVHS applications at all of these frequencies can be analyzed using ITS propagation models after certain modifications have been made. Modifications to these models were described in the Section 4 of this report. Some analyses to follow will involve far-field considerations, near-field considerations, or both.

5.1 Applications at Frequencies of 40 GHz and Above.

- 5.1.1. Automatic Collision Avoidance
 - a. Longitudinal Collision Avoidance Radar
 - b. Lateral Collision Avoidance Radar

5.2 Applications at the 5.8 GHz Band

- 5.2.1 Automatic Collision Avoidance
 - a. Data Link to coordinate evasive actions
- 5.2.2 Automatic Vehicle Identification
 - a. Two-way Communications
- 5.2.3 Automatic Vehicle Location
 - a. Two-way Communications
- 5.2.4 Driver/Vehicle Status Reporting
 - a. One-way Communications
 - b. Two-way Communications
- 5.2.5 Electronic Siren
 - a. One-way Communications
- 5.2.6 Electronic Credentials (Commercial)
 - a. Two-way Communications
- 5.2.7 Electronic Toll Collection
 - a. Two-way Communications
- 5.2.8 HAZMAT Access Control
 - a. Two-way Communications
- 5.2.9 HAZMAT Warning Beacon
 - a. Two-way Communications
- 5.2.10 In-vehicle Signing
 - a. One-way Communications
- 5.2.11 Parking Information
 - a. One-way Communications could be covered by cellular or PCS
- 5.2.12 Signal Priority (Emergency and Transit Vehicles)
 - a. One-way communication

- 5.2.13 Traffic Probing
 - a. Outbound poll to vehicle
 - b. Inbound response from vehicle

- 5.2.14 Transit Schedule Status Reporting
 - a. From Transit Vehicle to Dispatch

5.3 Applications at the 2.4 GHz Band

- 5.3.1 Automatic Vehicle Identification
 - a. Two-way Communications
- 5.3.2 Traffic Probing
 - a. Outbound Poll to Vehicle
 - b. Inbound Response from Vehicle

5.4 Applications at Frequencies Greater than 1 GHz (private microwave bands)

- 5.4.1 CCTV Communications and Control
 - a. Two-way Communications

5.5 Applications at Frequencies in the 902-928 MHz band

- 5.5.1 Automatic Vehicle Identification
 - a. One-way Communications
 - b. Two-way Communications
- 5.5.2 Automatic Vehicle Location
 - a. One-way Communications

5.6 Applications at Frequencies 150/450/800/900 MHz

- 5.6.1 Automatic Vehicle Location
 - a. Two-way Communications
- 5.6.2 CCTV Communications and Control
 - a. Two-way Communications
- 5.6.3 Changeable Message Sign Control
 - a. One-way Communications
- 5.6.4 Dispatching (Commercial, Emergency, Transit, Transit-Handicap)
 - a. Two-way Communications

- 5.65 Driver/Vehicle Status Reporting
 - a. One-way Communications
 - b. Two-way Communications
- 5.6.6 In-Road and Roadside Detector Reports
 - a. Wireline, Radio
- 5.67 Route Guidance (Centralized)
 - a. Two-way Communication RF
- 5.6.8 Traffic Signal Control
 - a. Wireline, Radio
- 5.6.9 Transit Schedule Status Reporting
 - a. From Transit Vehicle to Dispatch

5.7 Applications at 220 MHz

- 5.7.1 In-Vehicle Signing
 - a. One-way Communications
- 5.7.2 MAYDAY (Automatic) Air-bag Sensor
 - a. Two-way Communications
- 5.7.3 Terrain/Hazard Warnings
 - a. One-way Communications
- 5.7.4 Traffic Probing
 - a. Outbound Poll to Vehicle
 - b. Inbound Response from Vehicle
- 5.7.5 Variable Message Sign Control
 - a. One-way Communications

5.8 Applications in the FM Broadcast Band (88-108 MHz)

- 5.8.1 Changeable Message Sign Control
 - a. One-way Communications
- 5.8.2 Incident Reporting
 - a. Outbound to Vehicles
- 5.8.3 Traffic Probing
 - a. Outbound Poll to Vehicle

5.9 Other Systems, Applications, or Functions Not Included Above

One system under testing but not in the matrix is the Advanced Traveler Information System (ATIS) category. This is the AM subcarrier system for Colorado Rural ATIS system under development and testing by the Colorado Department of Transportation. The ranges involved will be fractions of a kilometer to many kilometers. In some cases this may involve near-field analysis. This system can be analyzed using ITS's ground-wave and sky-wave models, because it is in the AM broadcast band (550-1600 kHz).

Other systems under testing and or development by manufacturers include those found in the following report. Some of these frequencies are mentioned in the matrix and some are not. A report "Recommendations on Selection of Vehicle-to-Roadside Communications Standards for Commercial Vehicle Operations", prepared by The National Institute of Standards and Technology, Robot Systems Division discusses 15 proposed systems to be used for vehicle-to-roadside communications. Eleven of these systems are in the 902-928 MHz band. One of these systems requires operation at 49.86 MHz in addition to the 902-928 MHz band. Another of these systems operates at 845-850 MHz. Of the remaining three systems one specifies no frequency and the other two operate at 199 and 1.8 MHz. These systems operate at ranges from 4 to 5280 feet and under certain conditions would require special consideration for propagation analysis, because they are not in the far field of the antenna systems. Many of these must be treated as near field coupling problems. For the cases where far field separation is achieved the existing ITS propagation models can be used to predict IVHS system performance. Where the far field separation is not achieved, then near-field compensation modifications will have to be made to the model to perform a satisfactory analysis.

6. CONCLUSIONS AND RECOMMENDATIONS

The following tasks are recommended to upgrade ITS's propagation models to analyze IVHS and make performance predictions in the roadway environment. The actual analysis to determine feasibility of using the specific frequencies to perform specific IVHS functions described in Section 5 will be performed in Phase 2 of the propagation modeling in the roadway environment task.

Task 1: Modeling out-of-sight propagation

In this effort, we will modify our existing urban canyon models to take into account the propagation down side streets and multi-side streets. This task is composed of five phases.

Phase I: Cross streets propagation

Phase II: Propagation down multiple side streets

Phase III: Impedance edge and corner diffraction

Phase IV: Diffracted fields from corners to street to receiver

Phase V: Multiple diffractions from closely spaced corners and objects

Task 2: Measurements of out-of-sight propagation

In this task, we will undertake a measurement campaign to measure signal levels for out-of-sight (OOS) propagation in different urban canyon settings.

Task 3 : Propagation over rough streets

In this task, we will develop a set of curves for the magnitude and phase of the reflection coefficient for typical or realistic roughness dimensions that would be countered in an IVHS setting. These reflection coefficients for a non-smooth street could then be incorporated into the existing propagation model. The second phase of this task will be to study the Doppler effects of signal scattering from a rough moving street.

Task 4: Optimal antenna height

In this task we will investigate what might be the optimal transmitter and receiver height for an IVHS system.

Task 5: Propagation down roads in thickly forested areas

In this task, the expression listed in the report for propagation through foliage can be incorporated into the propagation model. We are proposing to experimentally determine the reflection coefficients from a forest/air interface. Another part of this effort is to theoretically investigate the error that occurs in calculating the reflection coefficient by not considering the correction as mentioned above.

Task 6: Propagation through tunnels and bridges

The best way to approach this type of propagation environment is not entirely clear, so part of this task will be to investigate different techniques to determine the best way to model propagation through tunnels and bridges.

Task 7: Propagation through buildings in urban canyons

An experimental effort similar to that done by Alexander [51] and Seidel [53] for the indoor channel will be performed on various urban canyon settings, in order to accurately characterize the $1/r^2$ propagation loss through different types of buildings. In this effort the straight line propagation through the building model for the multiple side street scenario will be incorporated into PCSACM. Once the model is complete, we will then undertake a measurement campaign to measure signal levels for out-of-sight (OOS) propagation down multiple side streets. These measurements may then be used to validate the model.

Task 8: Compensation for near-field and close-in propagation distances

The models described in Section 3 of this report will need some compensation to allow for near-field and inductive field coupling in situations where the specific IVHS functions are operating at distances that are so close as to make a far-field analysis an invalid approach for performance prediction. This task will investigate approaches to take this near-field coupling into account.

These tasks can be performed separately. The FHWA can select which of these tasks they would like to see performed in preference to the others. Tasks 1,2,3,6 and 8 are considered essential to performing an adequate analysis effort for determining suitability of the proposed frequencies and evaluating IVHS system performance for FHWA Operational Tests. These tasks will be performed after approval by FHWA in the second phase of the “Propagation Modeling in The Roadway Environment” effort.

REFERENCE

- [1] Y. Yamaguchi, T Takeo, and T. streets crowded with pedestrians”, IEEE Transactions on Electromagnetic Compatibility, vol. 30, no. 2, pp. 130-136, 1988.
- [2] C. Bergljung and L. G. Olsson, “Rigorous diffraction theory applied to street microcell propagation”, IEEE Global Telecommunication Conference, Dec. 2-5, pp. 1292- 1296, 1991.
- [3] T. Takeuchi, M. Sako, and Susumu Yoshida, “Multipath delay prediction on a workstation for urban mobile radio environment”, IEEE Global Telecommunication Conference, Dec. 2-5, pp. 308-1312, 1991.
- [4] A J. Rustako, N. Amitay, G. J. Owens, and R. S. Roman, “Radio propagation at microwave frequencies for line-of-sight microcellular mobile and personal communications”, IEEE Trans. on Vehicular Technology, vol. 40, no. 1, pp. 203-210, 1991.
- [5] L. R. Maciel, H. L. Bertoni and Howard H. Xia, “Unified approach to prediction of propagation over buildings for all ranges of base station antenna height”, IEEE Trans. on Vehicular Technology, vol.47 no. 1, pp. 41-45, 1993.
- [6] E. Violette, R Espeland, and K.C. Allen, “Millimeter-Wave Propagation Characteristics and Channel Performance for Urban-Suburban Environments”, NTIA report 88-239, 1988.
- [7] K. C. Allen, “A model of millimeter-wave propagation for personal communication networks in urban settings”, NTIA report 91-275, 1991.
- [8] N. De Minco, “Automated Performance Analysis Model for Ground-Wave Communication Systems”, NTIA report 86-209, 1989.
- [9] L.R. Teters, J.L. Lloyd, G.W. Haydon, and D.L. Lucas, ” Estimating the Performance of Telecommunication Systems Using the Ionospheric Transmission Channel”, NTIA report 83-127, 1983.
- [10] A. G. Longley and P.L. Rice, “Prediction of Tropospheric Radio Transmission Loss Over Irregular Terrain”, ESSA Technical Report ERL 79-ITS 67, 1968
- [11] G.A. Hufford, A.G. Longley, and W.AKissick." A Guide to the Use of the ITS Irregular Terrain Model in the Area Prediction Mode”, NTIA report 82- 100, 1982.
- [12] K.C. Allen,“EHF Telecommunication System Engineering Model”, NTIA report 86-1 92, 1986.
- [13] H.JLiebe,“An Atmospheric Millimeter Wave Propagation Model”, NTIA report 83-127, 1983.

- [14] H. J. Liebe, "MPM- An Atmospheric Millimeter Wave Propagation Model", International Journal of Infrared and Millimeter Waves, Vol. 10, No. 6, 1989
- [15] J. Washburn, G. Hand, M. Laflin, and N. Kuester, "Area coverage model for urban microcells", NTIA report in progress.
- [16] V. Erceg, S. Ghassemzadeh, M. Taylor, D. Li, and D. L. Schilling, "Urban/Suburban Out-of-Sight propagation modeling", IEEE Communications Magazine, pp. 56-61, June 1992.
- [17] T. S. Yim and T. H. Siang, "A new propagation model for a street scene for microcellular communications", International Electromagnetic Compatibility Symposium, Singapore, Dec. 7-9, pp. 200-207, 1992.
- [18] L. Boithias, Radio Wave Propagation, McGraw-Hill, N.Y., N.Y., 1987.
- [19] R. J. Doviak and D. S. Zrnicek, Doppler Radar and Weather Observations, Second Edition, Academic Press San Diego, Ca, 1993.
- [20] S. Shibuya, A Basic Atlas of Radio-Wave Propagation' New York: John Wiley & Sons, 1987, pp. 332-368.
- [21] R. J. Achatz, "Performance prediction of direct sequence modems in the indoor channel," NTIA report in progress.
- [22] W. B. Westphal and A. Sils, "Dielectric Constant and loss data", Massachusetts Institute of Technology, Technical Report AFML-TR-72-39, April, 1972.
- [23] A. N. Sivov, "Reflection of electromagnetic waves from corrugated surface with small period", Radiotekh. Elektron., vol. 9, pp. 1821-1827, 1964 [in Russian; Engl. transl. in Radio Eng. Electron., Phys., vol. 9, 1509-1515, 1964]
- [24] L. A. Vainshtein (Wainstein), "On the electrodynamic theory of grids", in Elektronika Bol'shikh Moshchnosti, vol. 2 (P. L. Kapitsa and L. A. Vainshtein, eds.). Moscow: Nauka, 1963, pp. 26-74 [in Russian; Engl. transl. in High-Power Electronics. Oxford: Pergamon Press, 1966, pp. 14-48].
- [25] M. A. Boit, "Lagrangian analysis of multiple scatter in acoustic and electromagnetic reflexion", Bull. Acad. Royale Cl. Sci., vol. 59, pp.153-169, 1973.
- [26] I. L. Verbitskiy, "The diffraction of a plane wave by a dense comb", Radio Eng. Electron. Phys, no. 3, pp. 41-46, 1976.
- [27] C. L. Holloway, "Edge and surface effects on conductor loss associated with planar circuits", MIMICAD technical report no. 12, Department of Electrical and Computer Engineering, University Colorado, Boulder, Colorado, chapter 3, 1992.

- [28] C. L. Holloway and E. F. Kuester, "The use of homogenization in deriving effective boundary conditions for perfectly conducting periodic surfaces," submitted to *Wave Motion*, 1994.
- [29] C. L. Holloway and E. F. Kuester, "Impedance type boundary conditions for both 2-dimensional and 3-dimensional periodic interfaces," submitted to *J. Electromagnetic Waves and Appl.*, 1994.
- [30] R. G. Brown, R. A. Sharpe, W. L. Hughes and R. E. Post, "Lines, Waves, and Antennas, The Ronald Press Comp., N.Y., N.Y., 1973
- [31] F. G. Bass and I. M. Fuks, *Wave scattering from Statistically Rough Surfaces*. Oxford: Pergamon Press, 1979, chapter 3.
- [32] P. Beckmann and A. Spizzichino, *The Scattering of Electromagnetic Waves from Rough Surfaces*. Not-wood, MA: Artech House, 1987.
- [33] J. R. Wait, "Perturbation analysis for reflection from two-dimensional periodic sea waves", *Radio Sci.*, vol. 6, pp. 387-391, 1971.
- [34] D. E. Barrick, "Theory of HF and VHF propagation across the rough sea., 1, The effective surface impedance for a slightly rough highly conducting medium at grazing incidence", *Radio Sci.*, vol. 6, pp. 517-526, 1971.
- [35] A. R. Wenzel, "Smoothed boundary conditions for randomly rough surfaces", *J. Math. Phys.*, vol. 15, pp. 3 17-323, 1974.
- [36] R. K. Rosich and J. R. Wait, "A general perturbation solution for reflection from two-dimensional periodic surfaces", *Radio Sci.*, vol. 12, pp. 719-729, 1977.
- [37] D. Maystre, O. Mata Mendez and A. Roger, "A new electromagnetic theory for scattering from shallow rough surfaces", *Optica Acta*, vol. 30, pp. 1707-1 723, 1983.
- [38] G. S. Brown, "A comparison of approximate theories for scattering from rough surfaces", *Wave Motion*, vol. 7, pp, 195-205, 1985.
- [39] A. Ishimaru, *Electromagnetic Wave Propagation, radiation, and scattering*, New Jersey: Prentice Hall, 199 1, chapter 7.
- [40] J. A. Kong, *Electromagnetic Wave Theory*, New York: John Wiley & Sons, 1986, chapter VI.
- [41] R. G. Kouyoumjian and P. H. Pathak, "A uniform geometrical theory of diffraction for an edge in a perfectly conducting surface", *Proceedings of the IEEE*, vol. 62, no. 11, pp. 1448-1461, 1974.

- [42] D. A. McNamara, C. W. I. Pistorius, and J. A. G. Malherbe, *Introduction to the Uniform Geometrical Theory of Diffraction*, Boston: Artech House, 1990.
- [43] G. D. Maliuzhinets, "Excitation, reflection and emission of surface waves from a wedge with given face impedances", *Sov. Phys. Dokl.*, vol. 3, no. 4, pp. 752-755, 1958.
- [44] R. J. Luebbers, "Finite conductivity uniform GTD versus knife edge diffraction in prediction of propagation path loss", *IEEE Trans. on Antenna and Propagation*, vol. 32, no. 1, pp. 70-76, 1984.
- [45] C. A. Balanis, *Advanced Engineering Electromagnetics*, New York: John Wiley & Sons, 1989, chapter 13.
- [46] P. H. Pathak and R. J. Marhefka, *Asymptotic High Frequency Methods for EM Antenna and Scattering Analysis*, course notes for an IEEE AP-S short course, June, 1991.
- [47] E. F. Violette, R. H. Espeland, K. C. Allen, and F. Schwering, "Urban millimeter wave propagation studies", *Research and Development Technical Report, CECOM-83-3*, U.S. Army Communications Electronics Command, Fort Monmouth, NJ 07703, Apr., 1983.
- [48] J. Brown and W. Jackson' "the properties of artificial dielectrics at centimetre wavelengths", *Proc. IEE (London)*, vol. 102B, pp. 11-16, 1955.
- [49] L. Lewin, "The electrical constants of a material loaded with spherical particles", *The Institution of Electrical Engineers*, vol. 94, pt. III, no. 27, Jan. 1947.
- [50] P. C. Waterman and N. E. Pedersen, "Electromagnetic scattering by periodic array of particles", *J. Appl. Phys.*, vol. 59, no. 8, pp. 2609-2618, 1986.
- [51] J. Brown' "Artificial dielectrics having refractive indices less than unity", *The Institution of Electrical Engineers*, no. 62, May 1953.
- [52] A. Carne and J. Brown' "Theory of reflections from the rodged-type artificial dielectric", *Proc. IEE (London)*, vol. 106, pt. B, pp. 107-115, 1959.
- [53] C. L. Holloway, "Reflections from an array of periodically spaced conducting scatterers", In preparation for both a journal and a NTIA publication.
- [54] M. D. Yacoub, *Foundations of Mobile Radio Engineering*, Boca Raton, FL: CRC Press, 1993.
- [55] W. C. Jakes, *Microwave Mobile Communications*, New York: John Wiley & Sons, 1974, pp. 110-113.
- [56] S. E. Alexander, "Characterizing buildings for propagation at 900 MHz," *Electronics Letters*, vol. 19, no. 20, p. 860, 29th Sept. 1983.

- [57] S. Y. Seidel and T. S. Rappaport, "914 Mhz path loss prediction models for indoor wireless communications in multifloored buildings," IEEE Trans. on Antennas and Propagation, vol. 40, no. 2, pp. 207-217, 1992.

TABLES

TABLE 1: Conductivity of various types of foliage (from Yacoub [54], page 87).

Foliage	$\sigma(\times 10^{-5})$	
	Dry	Wet
Bare tree branches	0.5-1	2-10
Deciduous, full leaf	1	5-20
Evergreen forest	2- 5	5-20
Thin jungle scrub	1-10	3-20
Dense rain forest	10-50	50

TABLE 2: Distance/Power laws for propagation through different types of buildings (obtained from Alexander [56]).

Building	Construction	Coverage 1 m W (<i>a</i>) distance	Distance/ power law (gradient)	Correlation (<i>h</i>)	Spread +/-dB (<i>c</i>)
1 offices	brick	17 m	3.9	0.97	8
2 " 1st floor*	brick	12 m	3.9	0.96	10
" gnd floor	"	12 m	3.9	0.96	6
3	brick/block/plasterboard. reinforced concrete shell	25 m	6.1	0.89	16
4 " gnd floor*	brick/plasterboard	> floor	5.3	0.99	1
1st		16 m	4.7	0.94	12
2nd		12 m	4.8	0.95	8
through floors	reinforced concrete floors	10 m	5.1	0.98	3
1, 2, 3,4,5					
5 offices 1st floor*	plasterboard with	27 m	6.2	0.95	9
gnd floor	metal support studding	8 m	31	0.93	6
6 laboratory	block plus some metal faced partitioning	20 m	6.5	0.96	8
7 offices	plasterboard	30 m within 60 m outside	2.8	0.75	16
8 "	plasterboard	32 m	3.7	0.96	7
9 "	steel	10 m	5.7	0.92	10
10 house	brick/breeze/plasterboard	> building	1.4	0.54	7
11 "	brick/breeze block		4.0	0.76	7
12 "	brick/breeze block		2.2	0.70	12
13 workshop	open plan	60 m	2.5	0.97	4
14 hangar	open plan	> building	1.2	0.99	1

FIGURES

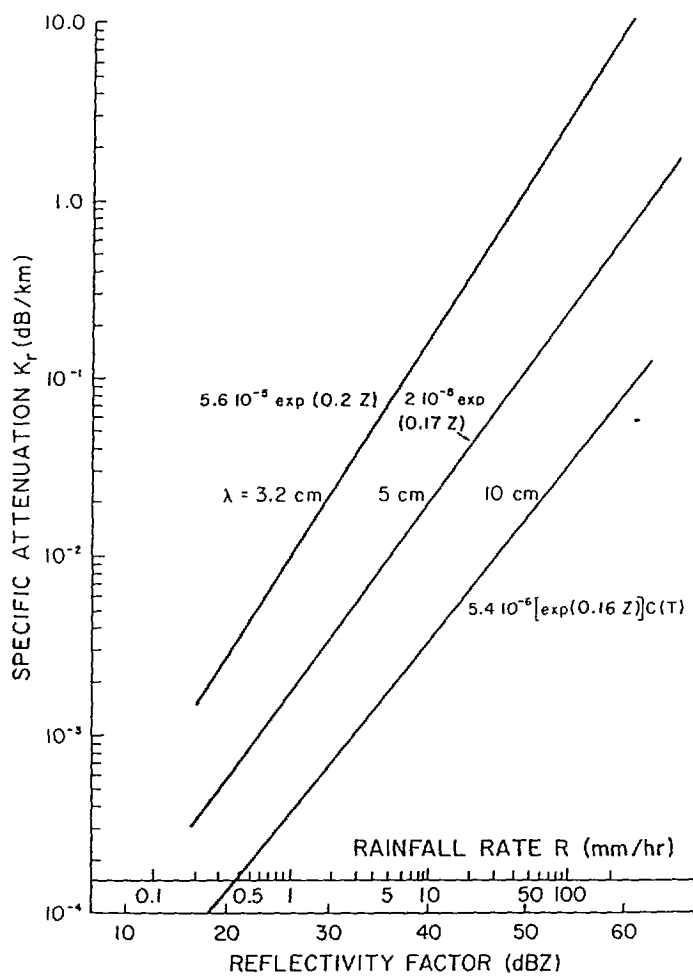


FIGURE 1: Attenuation due to different rainfall rate (from Doviak [19], page 42).

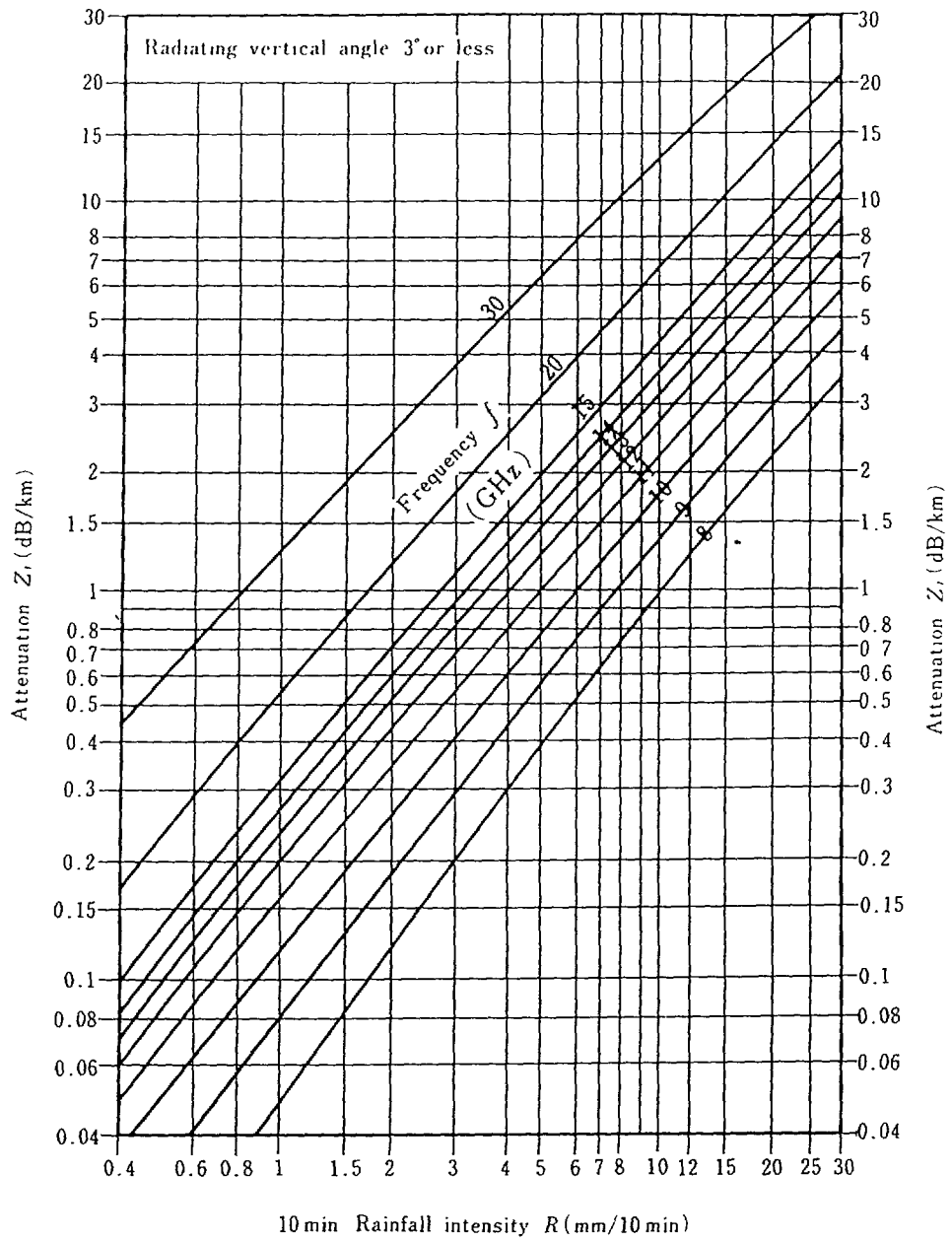


FIGURE 2: Attenuation due to different rainfall rate for GHz frequencies (from Shibuya [20], page 347).

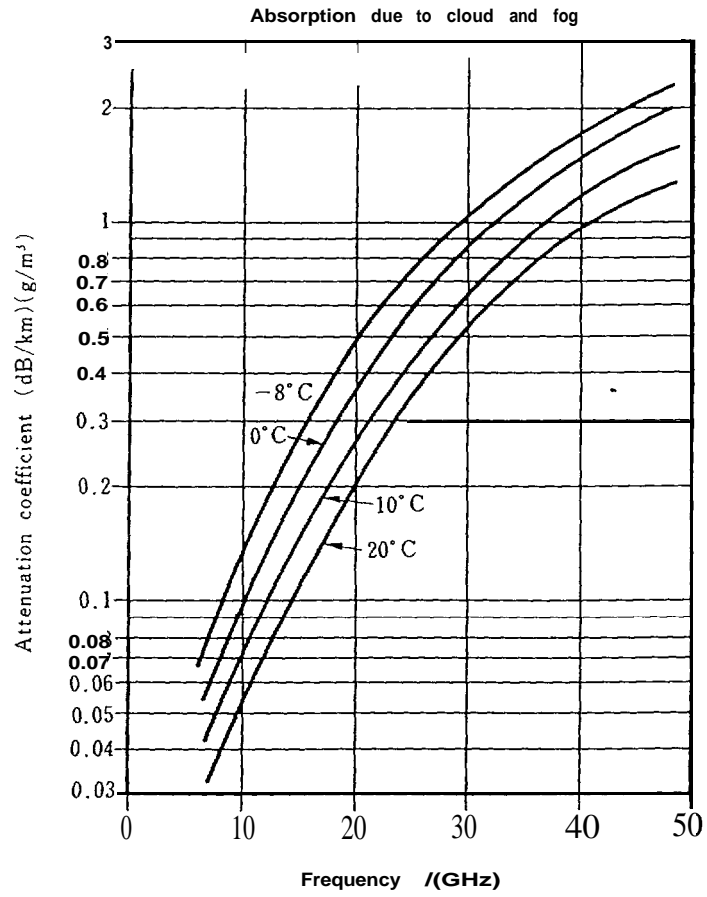


FIGURE 3: Attenuation due to cloud and fog (from Shibuya [20], page 345).

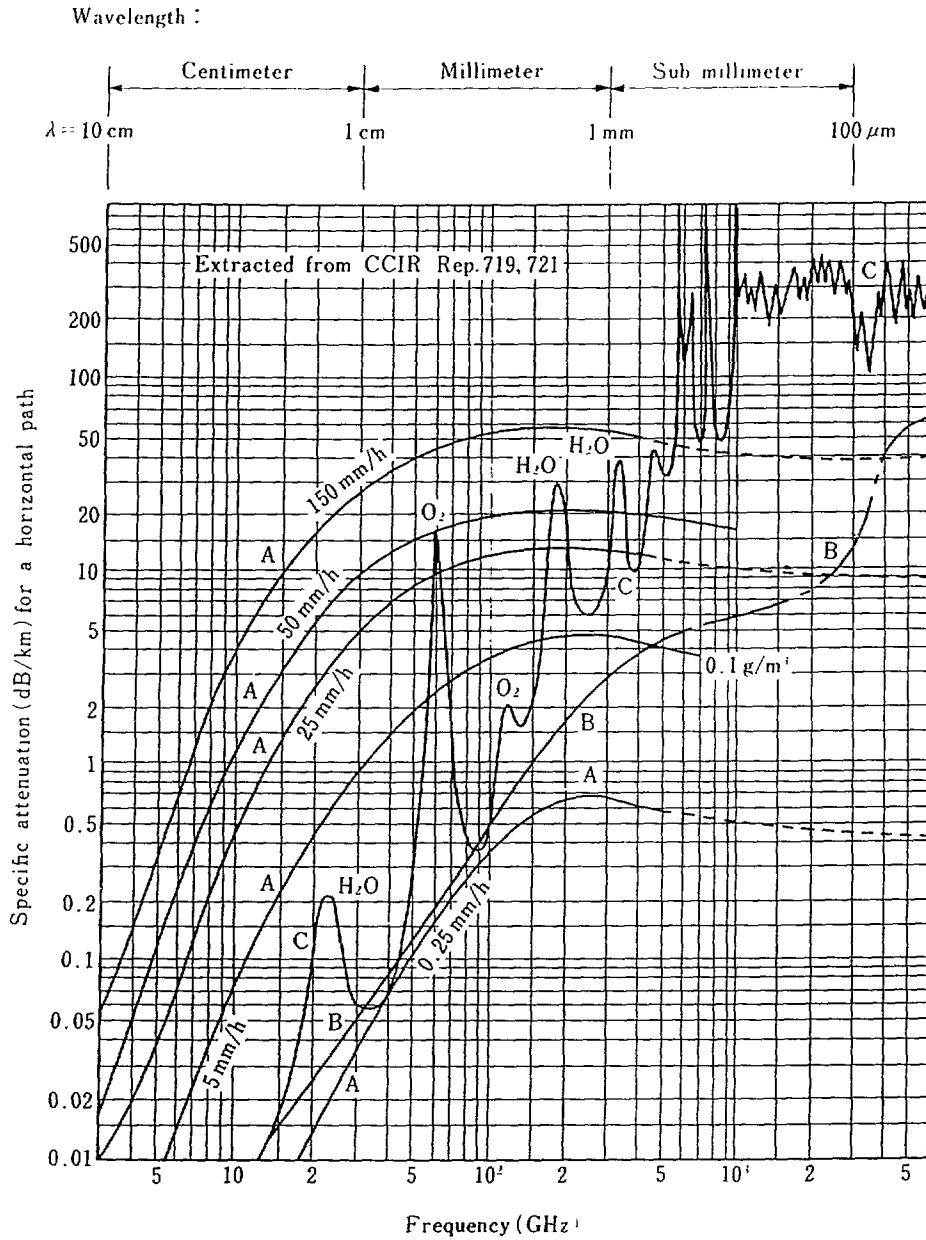


FIGURE 4: Attenuation due to gaseous constituents and precipitation (from Shibuya [20], page 368).

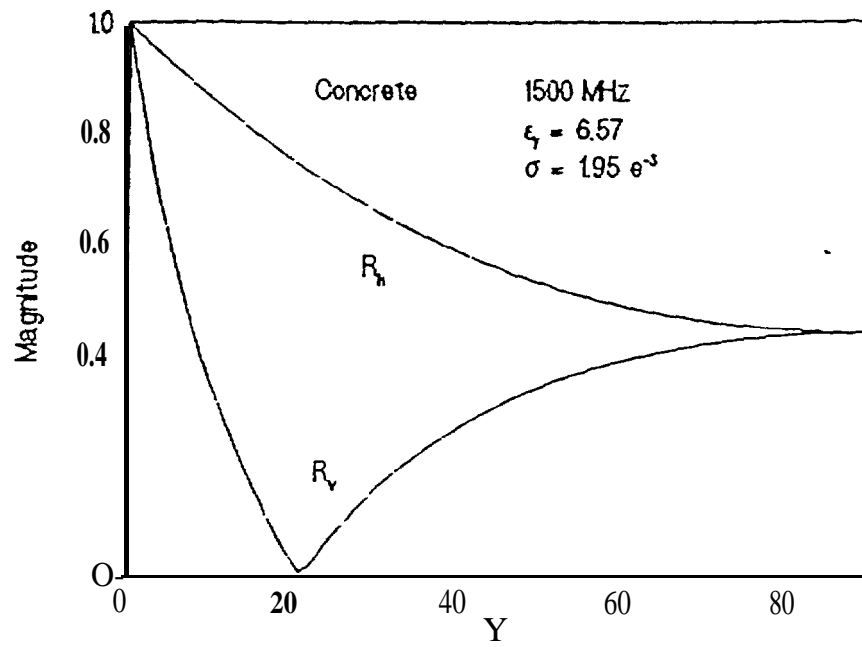


FIGURE 5: Reflection coefficients for both an E-polarized and H-polarized field incident onto an infinite thick slab of concrete (from Achatz [21], page 7).

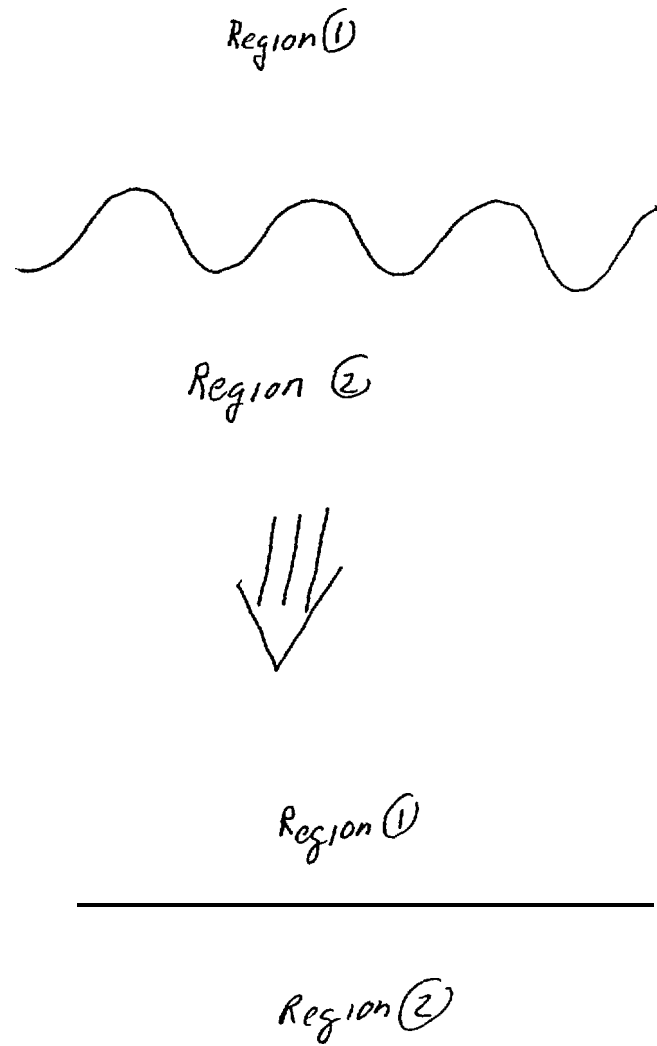


FIGURE 6: Replacement of the actual rough surface with a smooth surface, for which the effective boundary condition can be applied.

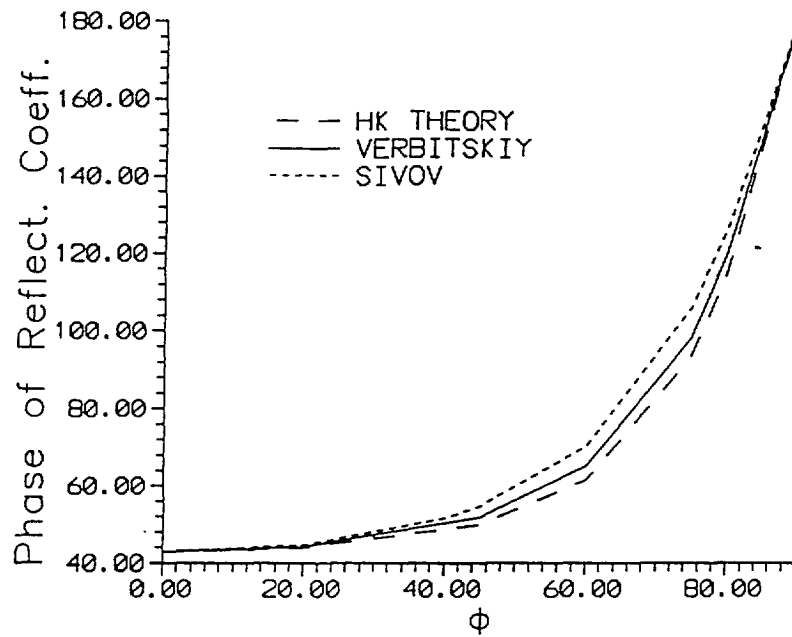


FIGURE 7: The phase of the reflection coefficient for a perfectly conducting rectangular profile, where the dimensions of the profile are small compared to a wavelength (from Holloway [27], page 169).

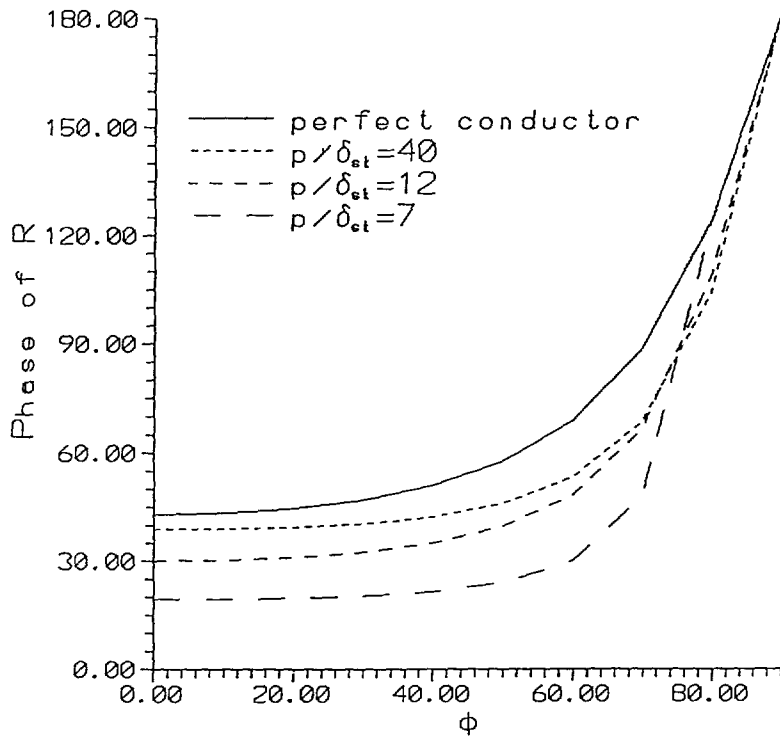


FIGURE 8: The phase of the reflection coefficient for a conducting rectangular profile, where the dimensions of the profile are small compared to a wavelength (from Holloway and Kuester [29]).

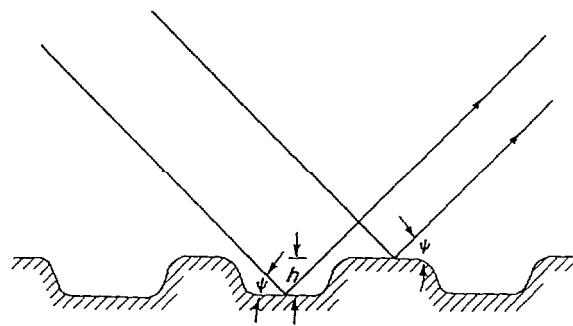


FIGURE 9: Illustration of the phase difference for a wave reflection off of a rough interface (from Brown et al. [30], page 409).

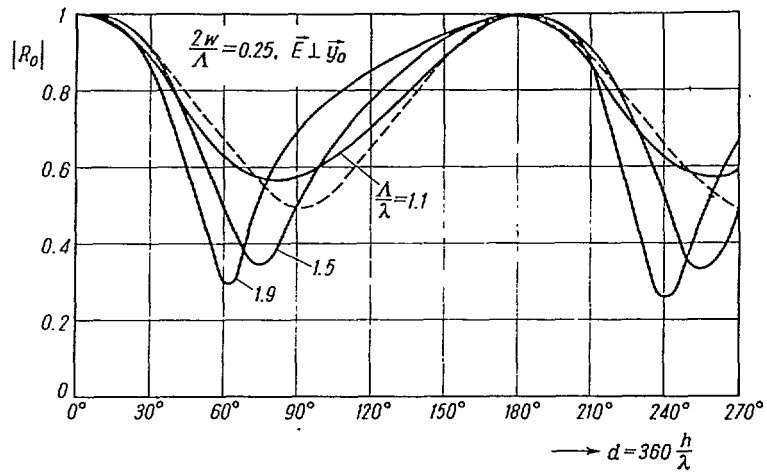


FIGURE 10: Reflections for a rectangular corrugation as a function of "electrical depth" $d = 360 h/\lambda$, where w is the width of the rough profile, h is the height of the profile and " λ " is the period of the profile. Lateral polarization, normal incidence, $2w/\lambda = 0.25$ (from [32], page 62).

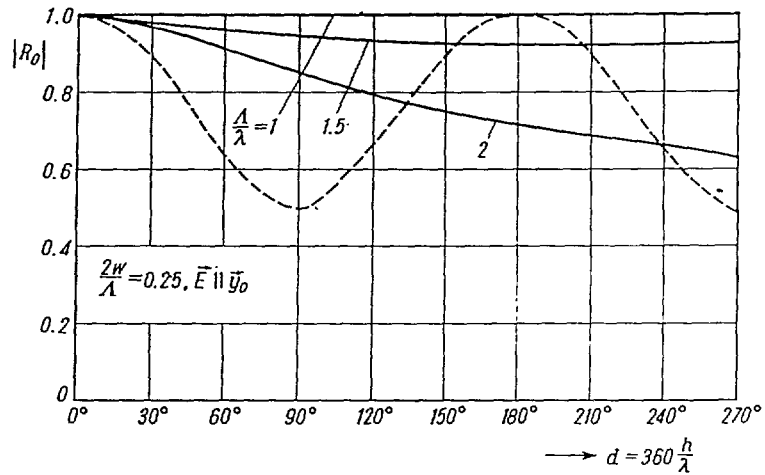


FIGURE 11: Reflections for a rectangular corrugation as a function of "electrical depth" $d = 360 h/\lambda$, where w is the width of the rough profile, h is the height of the profile and " λ " is the period of the profile. Longitudinal polarization, normal incidence, $2 w/\lambda = 0.25$ (from [32], page 64).

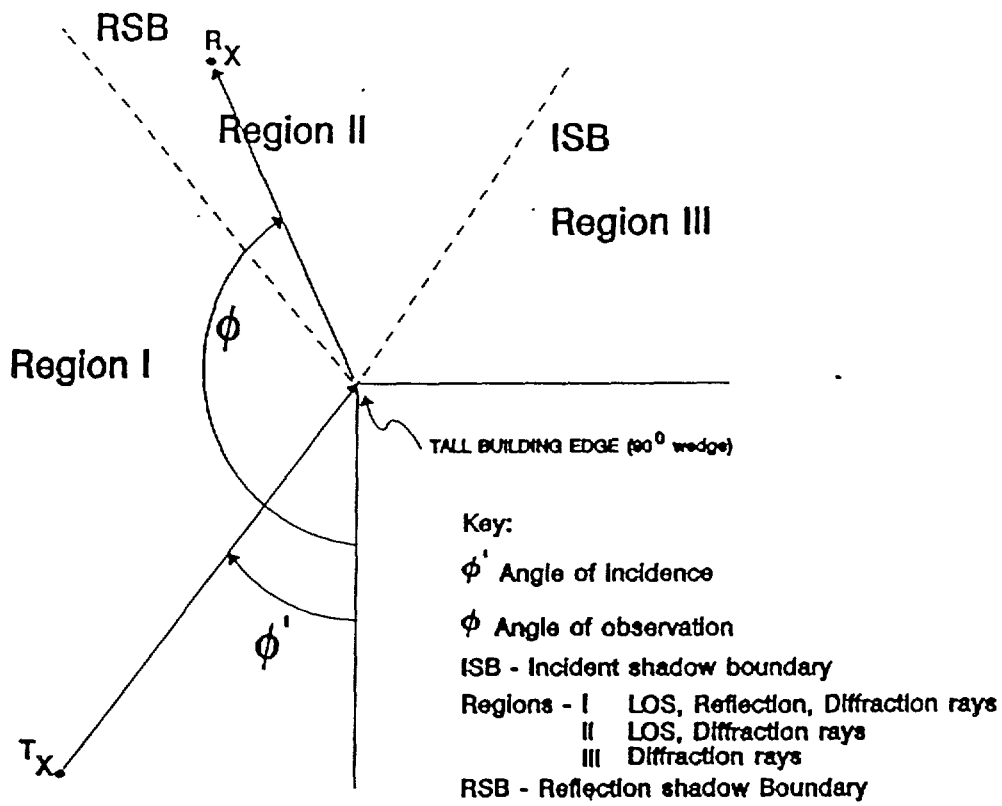


FIGURE 12: Diffraction of a ray by a corner.

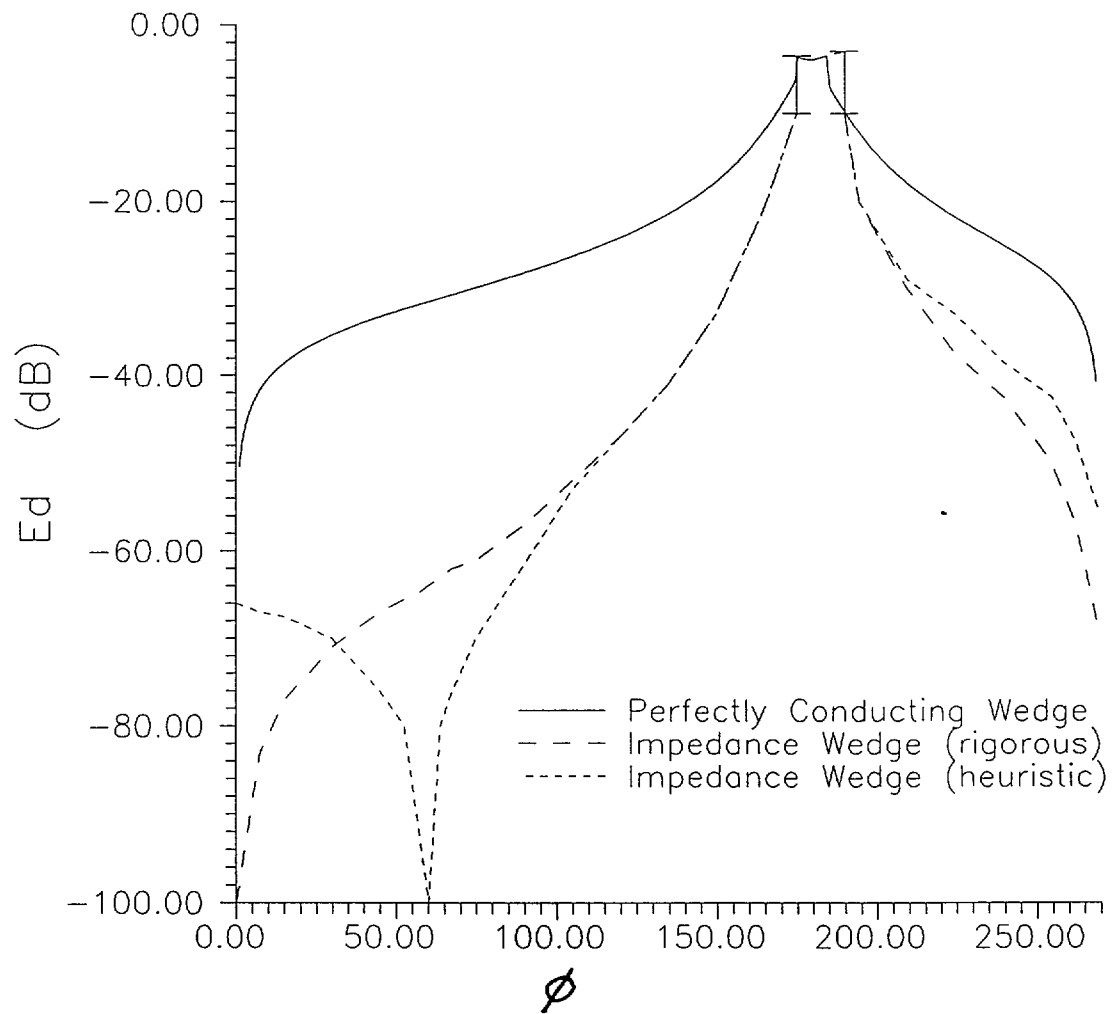


FIGURE 13: A comparison of the diffracted fields from a perfectly conducting corner to the diffracted field assuming a impedance corner using both the rigorous expression (Maliuzhinets [43]) and the heuristic expression (Luebbers [44]). These results are for a source location of $\phi = 5$ degrees.

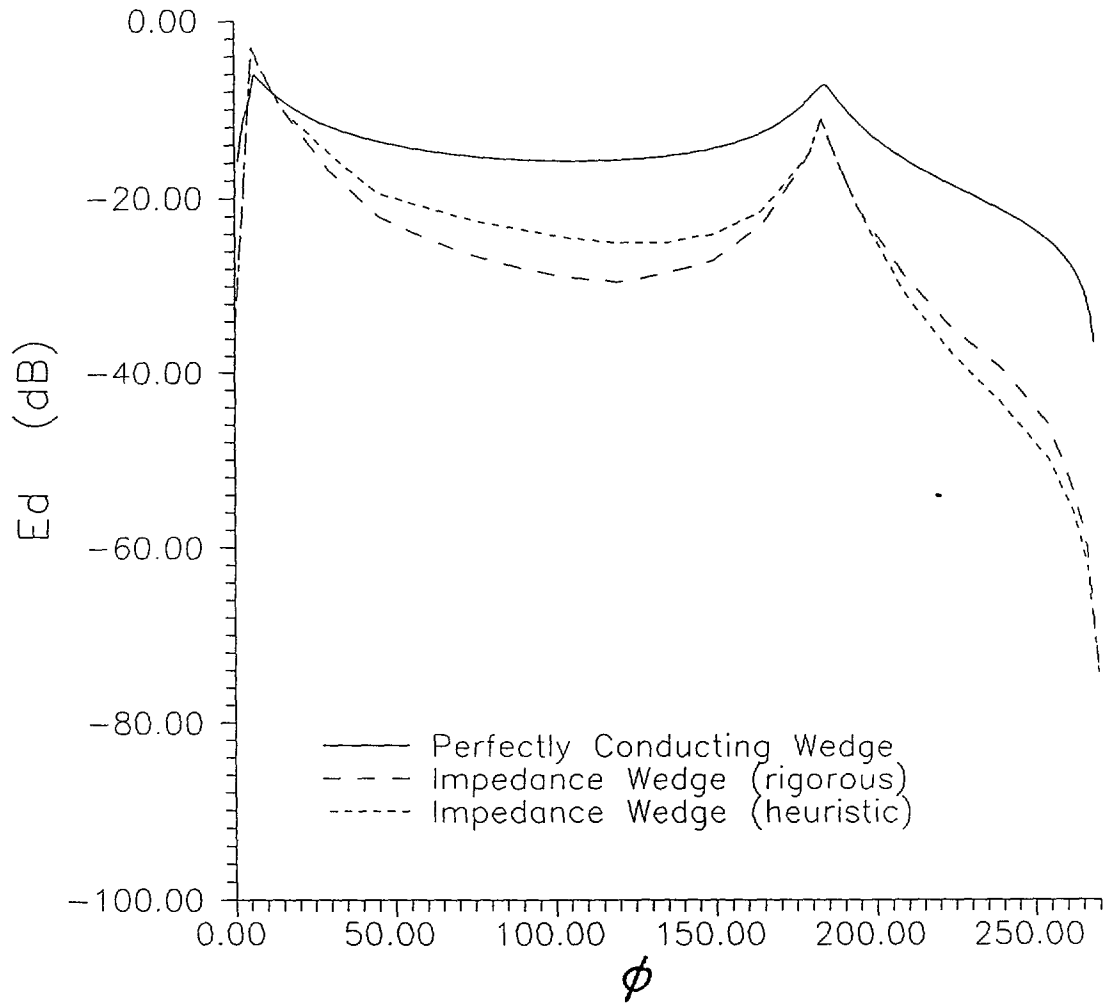


FIGURE 14: A comparison of the diffracted fields from a perfectly conducting corner to the diffracted field assuming a impedance corner using both the rigorous expression (Maliuzhinets [43]) and the heuristic expression (Luebbers [44]). These results are for a source location of $\phi = 17$ degrees.

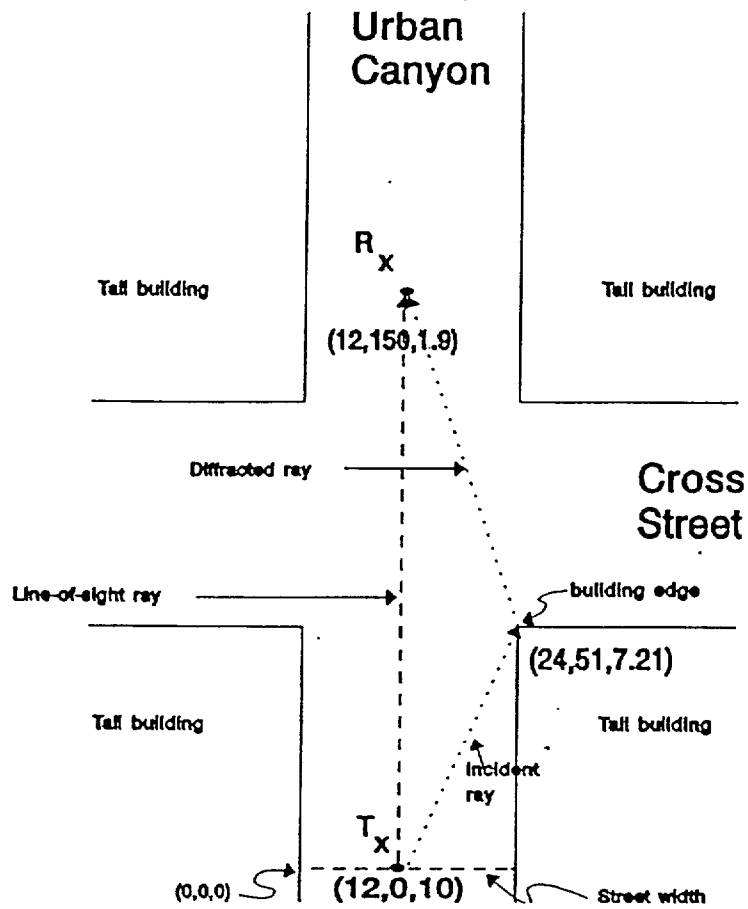


FIGURE 15: Urban canyon geometry (from [15], page 6).

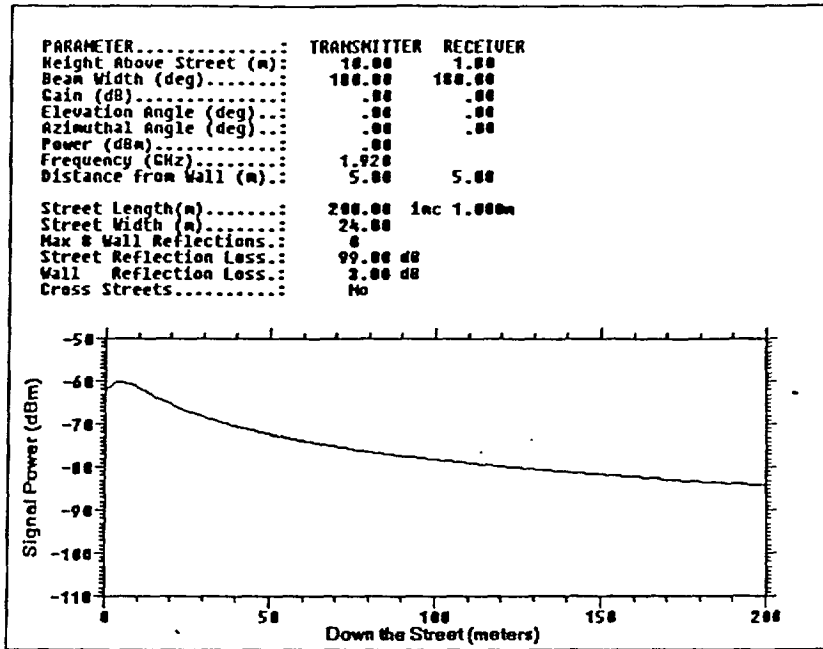


FIGURE 16: Example of a range scan for the signal levels in an urban canyon for line-of-sight propagation for free space loss only (from [15], page 34).

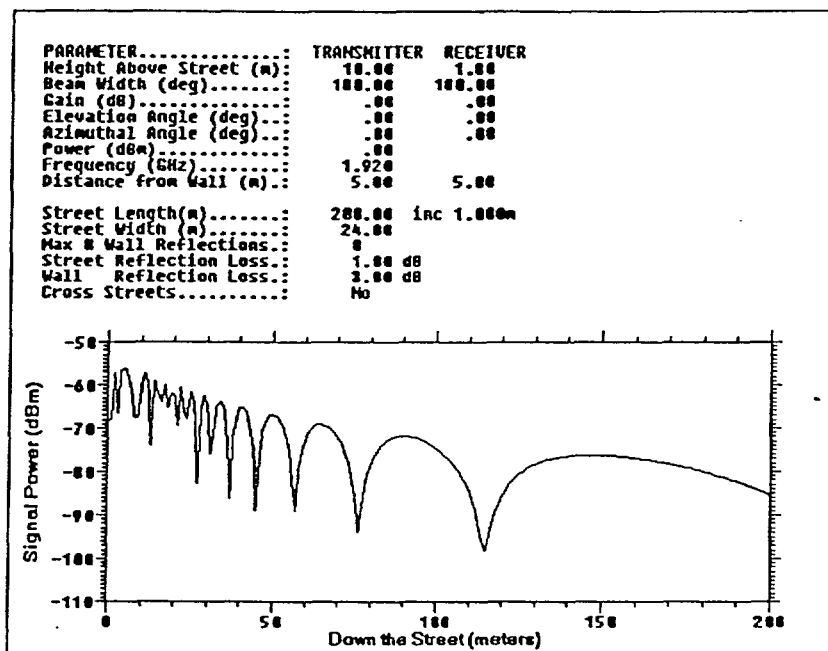


FIGURE 17: Example of a range scan for the signal levels in an urban canyon for line-of-sight propagation with losses due to free space and 1 street reflection (from [15], page 34).

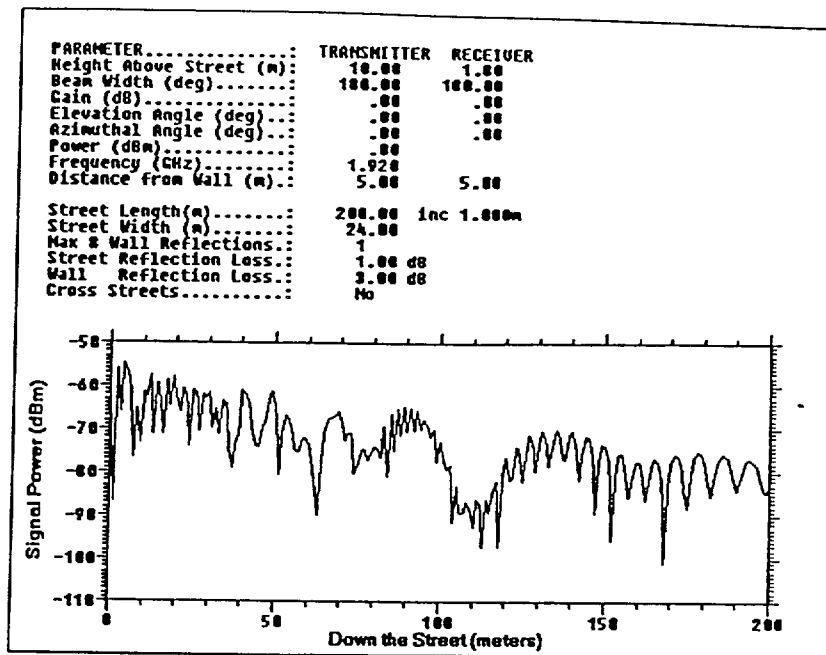


FIGURE 18: Example of a range scan for the signal levels in an urban canyon for line-of-sight propagation with losses due to free space, 1 street reflection, and 1 wall reflection (from [15], page 35).

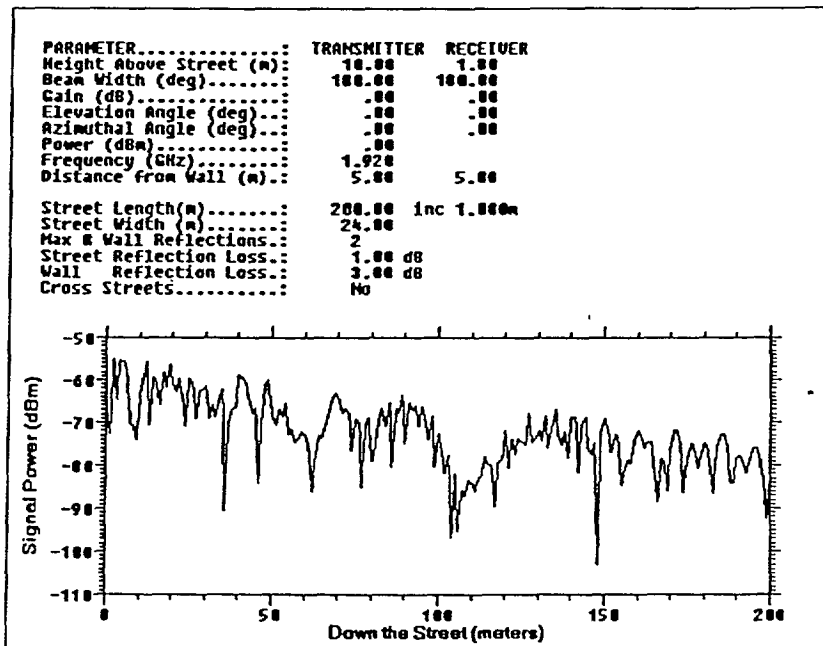


FIGURE 19: Example of a range scan for the signal levels in an urban canyon for line-of-sight propagation with losses due to free space, 1 street reflection, and 2 wall reflections (from [15], page 35).

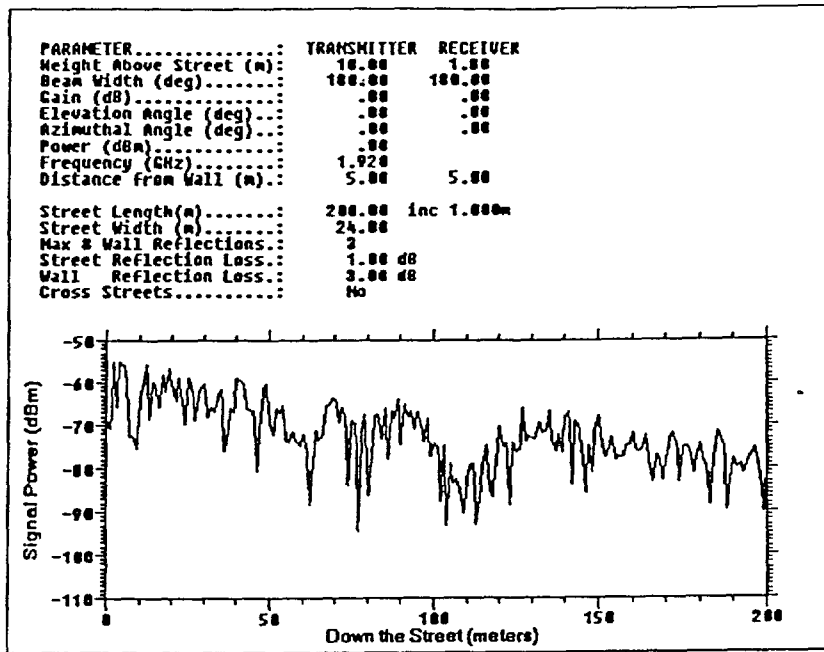


FIGURE 20: Example of a range scan for the signal levels in an urban canyon for line-of-sight propagation with losses due to free space, 1 street reflection, and 3 wall reflections (from [15], page 36).

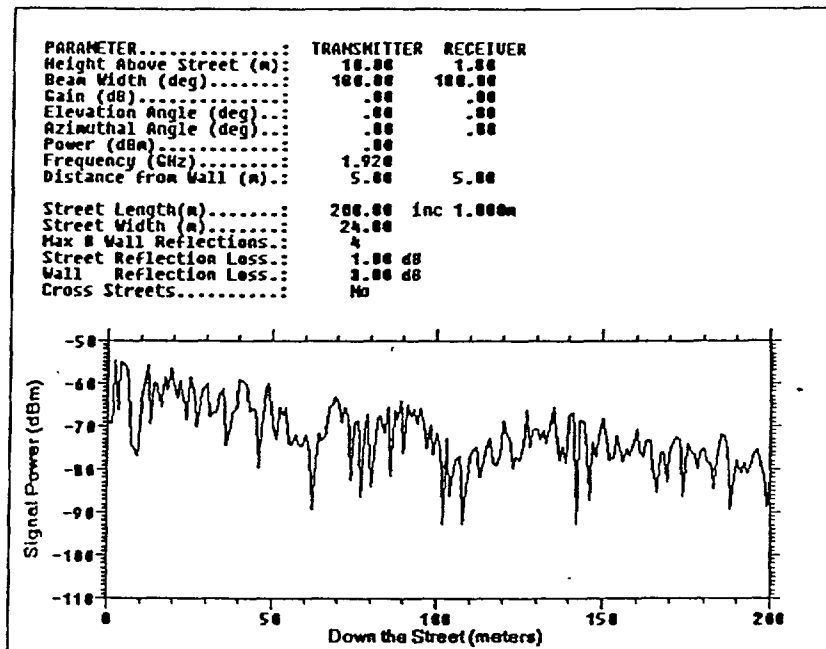


FIGURE 21: Example of a range scan for the signal levels in an urban canyon for line-of-sight propagation with losses due to free space, 1 street reflection, and 4 wall reflections (from [15], page 36).

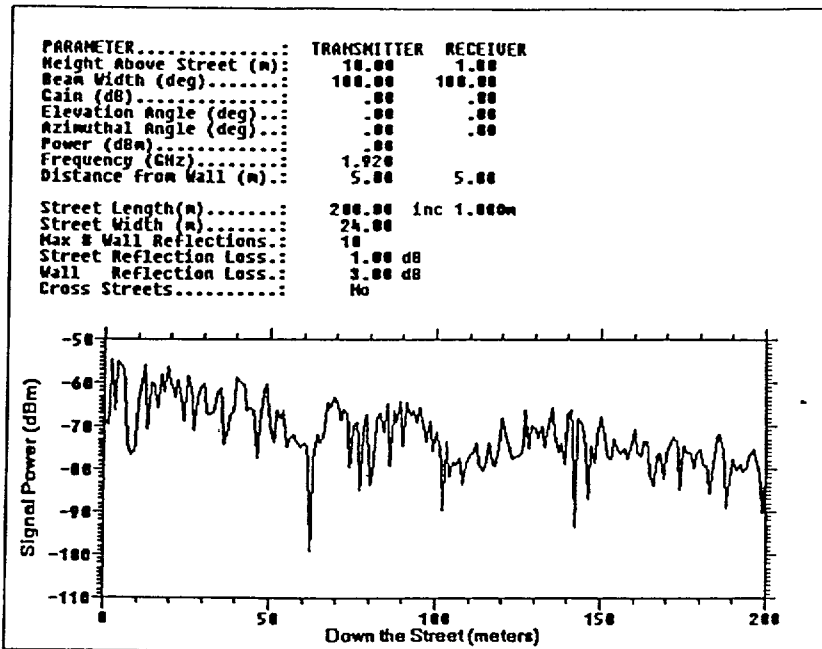


FIGURE 22: Example of a range scan for the signal levels in an urban canyon for line-of-sight propagation with losses due to free space, 1 street reflection, and 10 wall reflections (from [15], page 37).

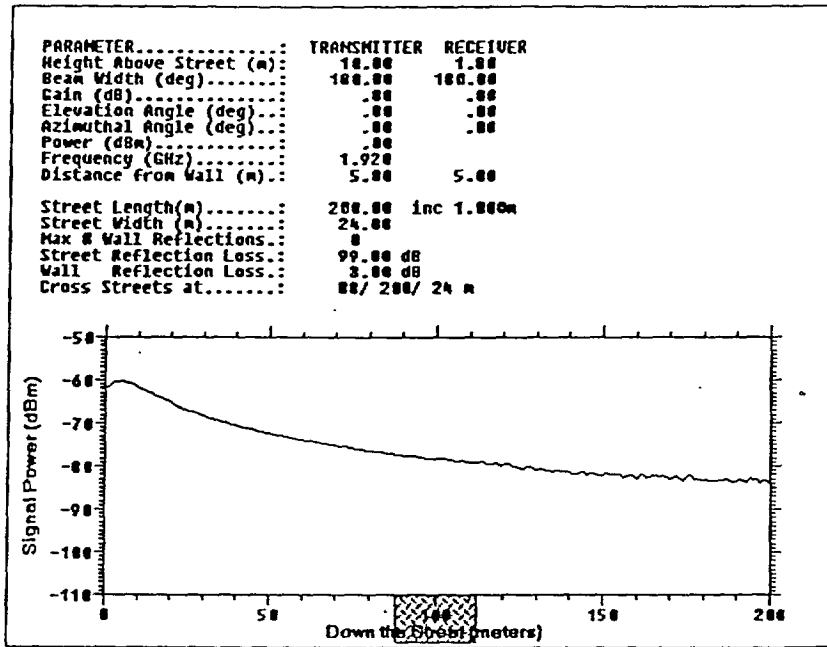


FIGURE 23: Example of a range scan for the signal levels in an urban canyon with one cross street for line-of-sight propagation for free space loss only (from [15], page 37).

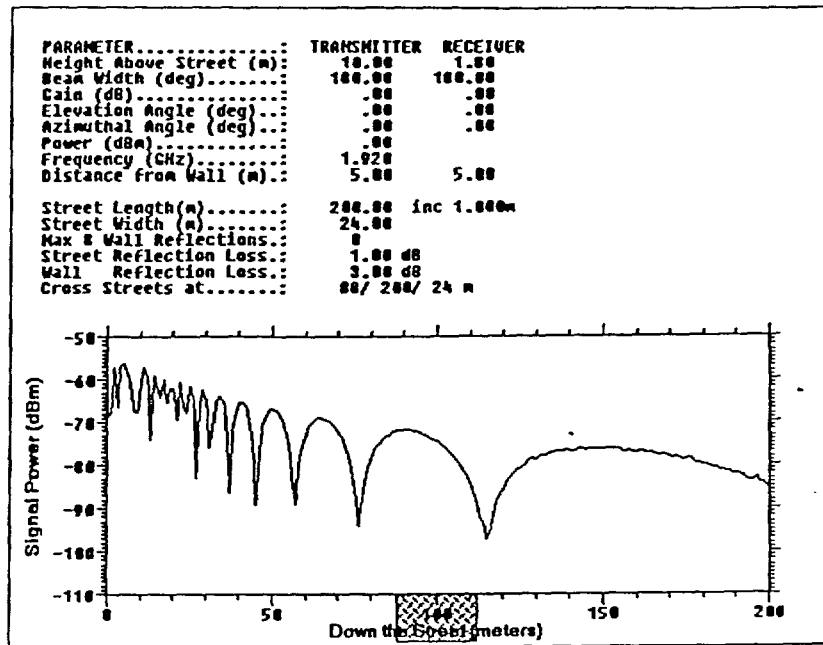


FIGURE 24: Example of a range scan for the signal levels in an urban canyon with one cross street for line-of-sight propagation with losses due to free space and 1 street reflection (from [15], page 38).

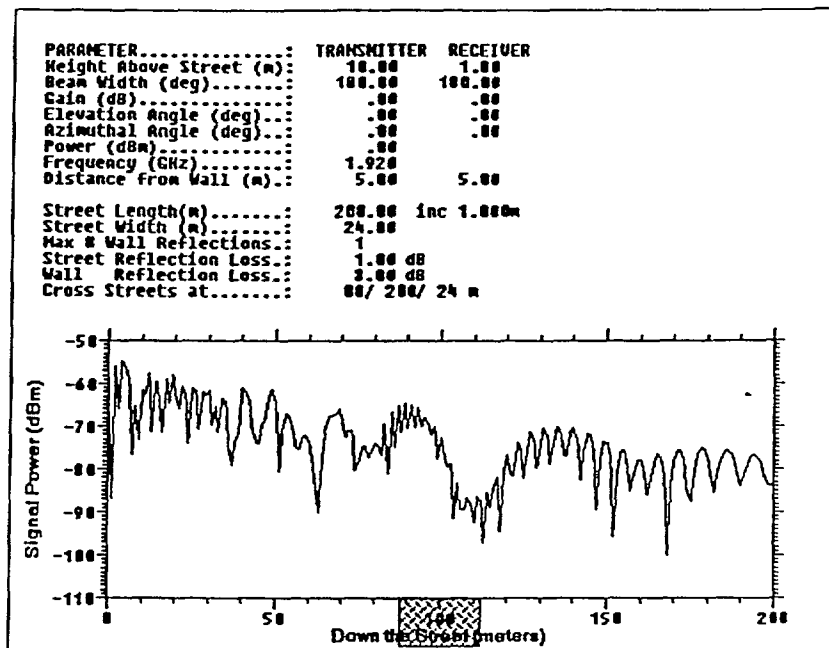


FIGURE 25: Example of a range scan for the signal levels in an urban canyon with one cross street for line-of-sight propagation with losses due to free space, 1 street reflection, and 1 wall reflection (from [15], page 38).

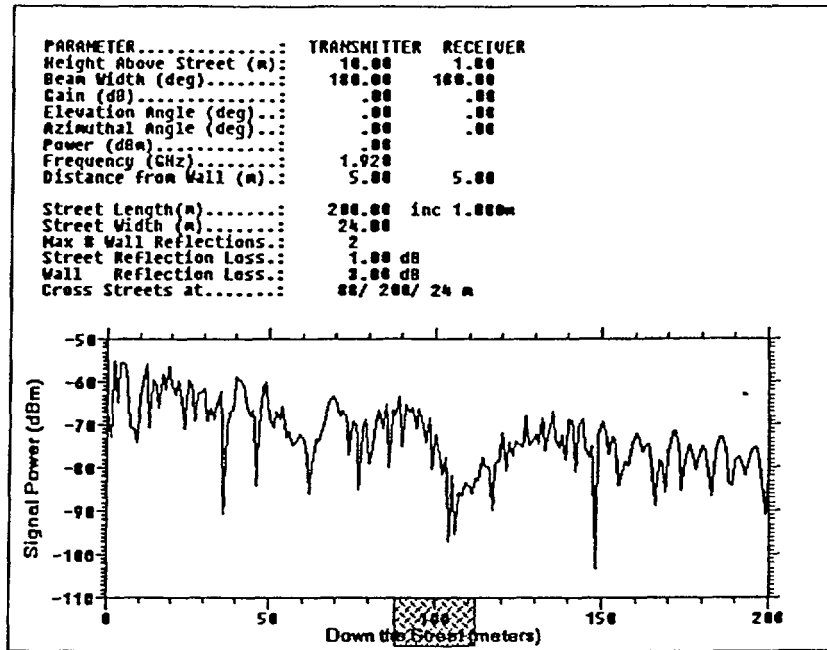


FIGURE 26: Example of a range scan for the signal levels in an urban canyon with one cross street for line-of-sight propagation with losses due to free space, 1 street reflection, and 2 wall reflections (from [15], page 39).

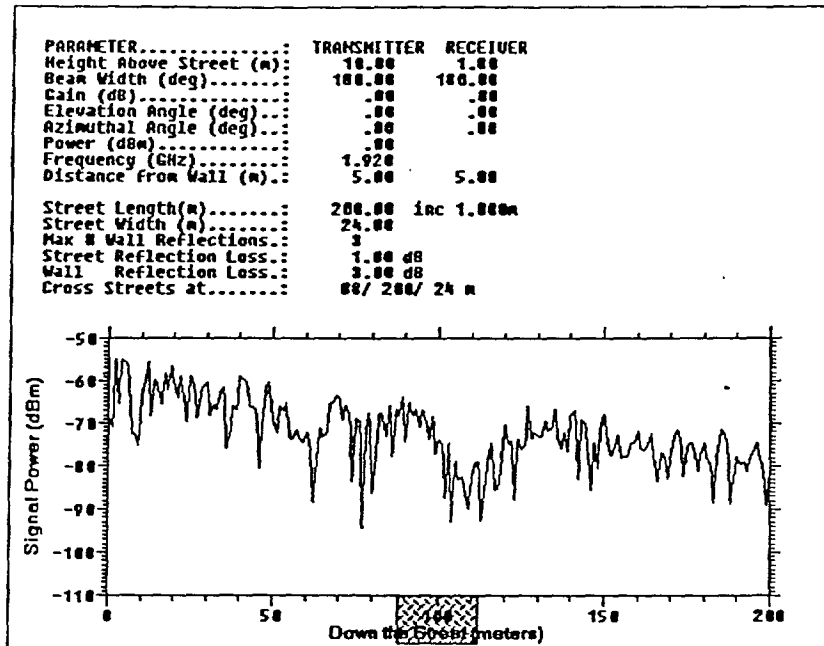


FIGURE 27: Example of a range scan for the signal levels in an urban canyon with one cross street for line-of-sight propagation with losses due to free space, 1 street reflection, and 3 wall reflections (from [15], page 39).

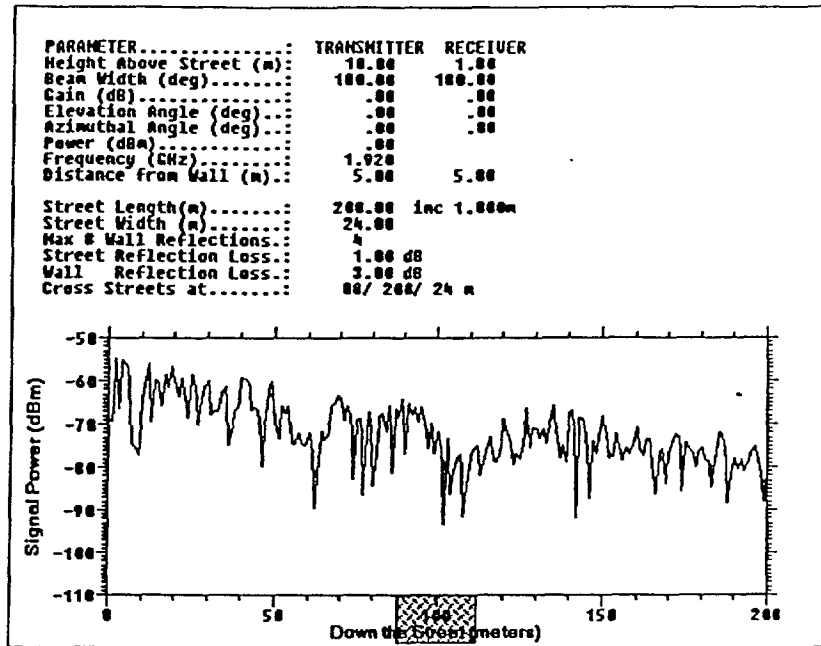


FIGURE 28: Example of a range scan for the signal levels in an urban canyon with one cross street for line-of-sight propagation with losses due to free space, 1 street reflection, and 4 wall reflections (from [15], page 40).

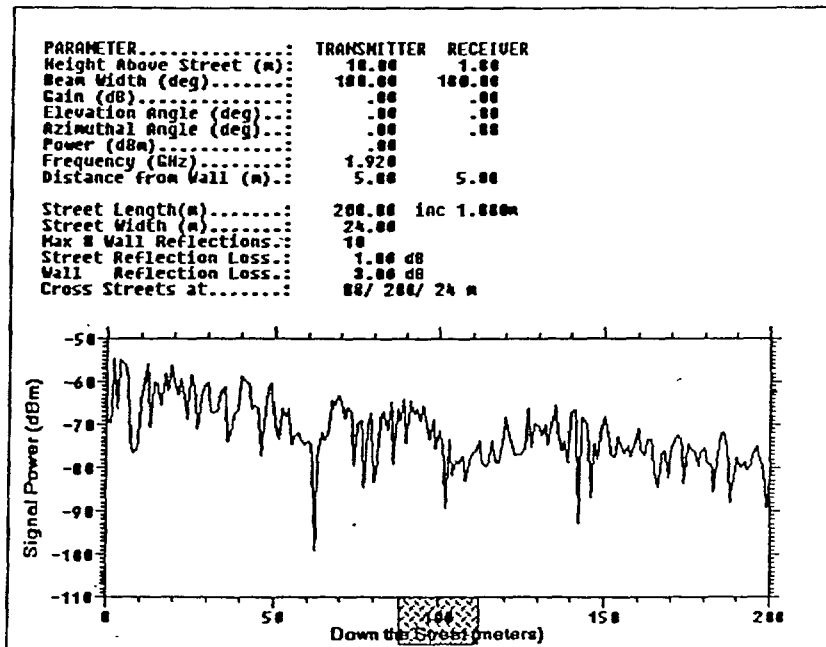


FIGURE 29: Example of a range scan for the signal levels in an urban canyon with one cross street for line-of-sight propagation with losses due to free space, 1 street reflection, and 10 wall reflections (from [15], page 40).

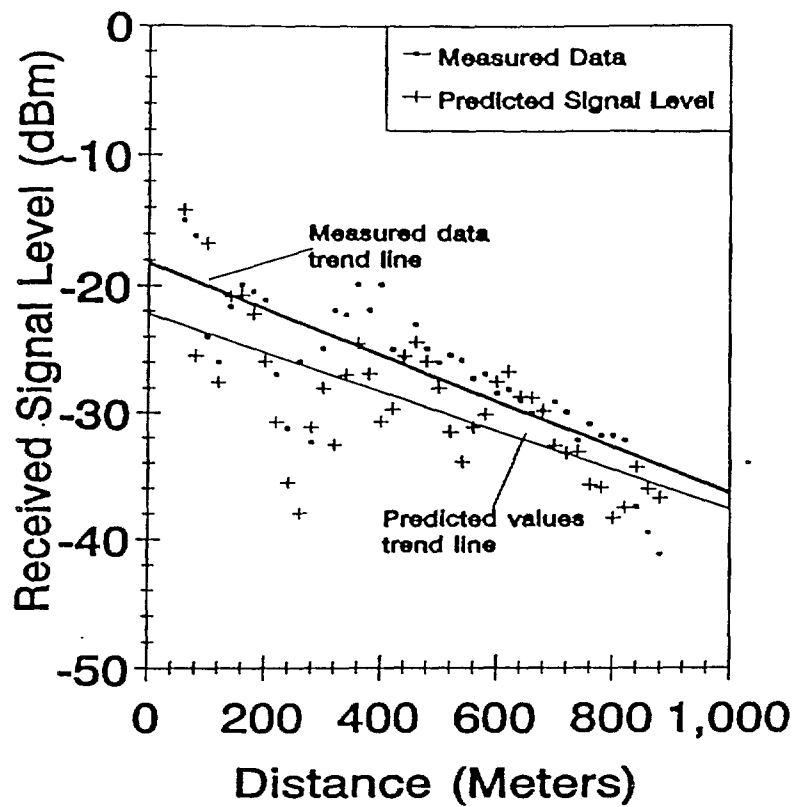


FIGURE 30: Range scans at 9.6 GHz of PCSACM predictions and measured data taken in an urban canyon in Denver, Colorado (from [15], page 41).

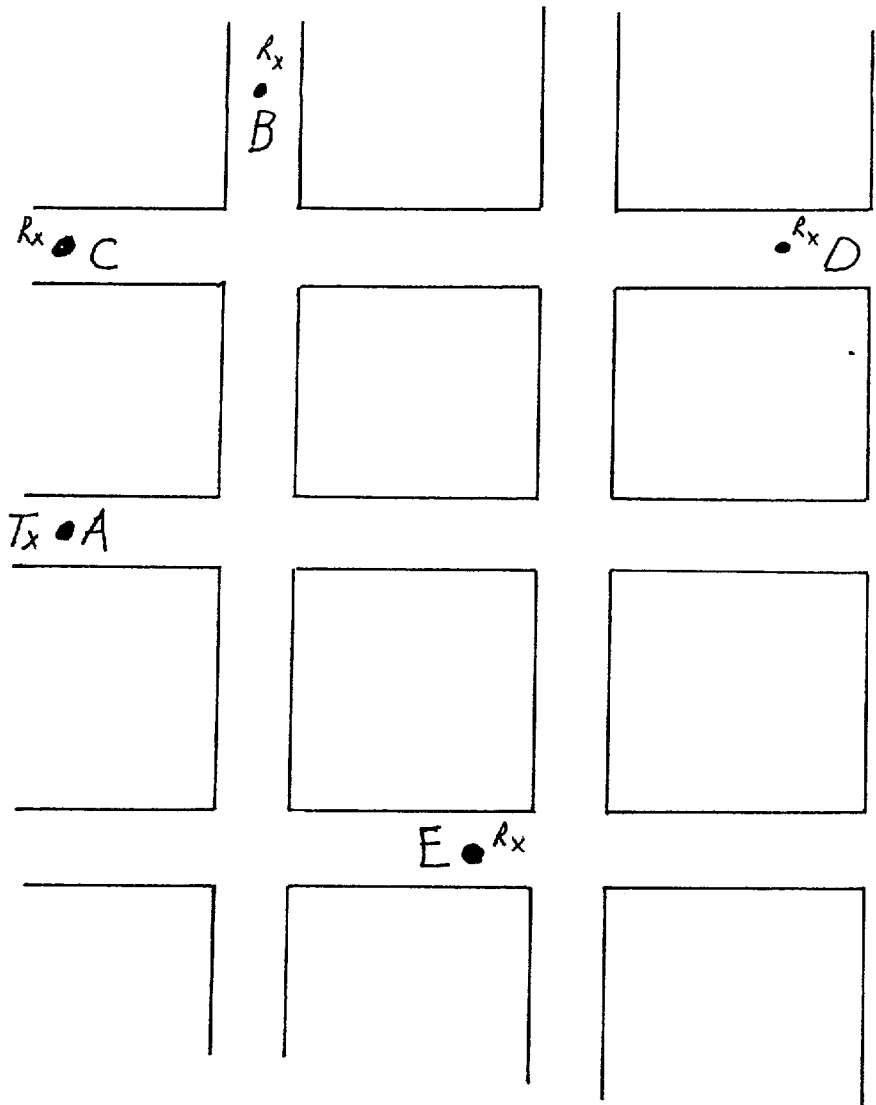


FIGURE 31: Illustration of side street receiver locations.

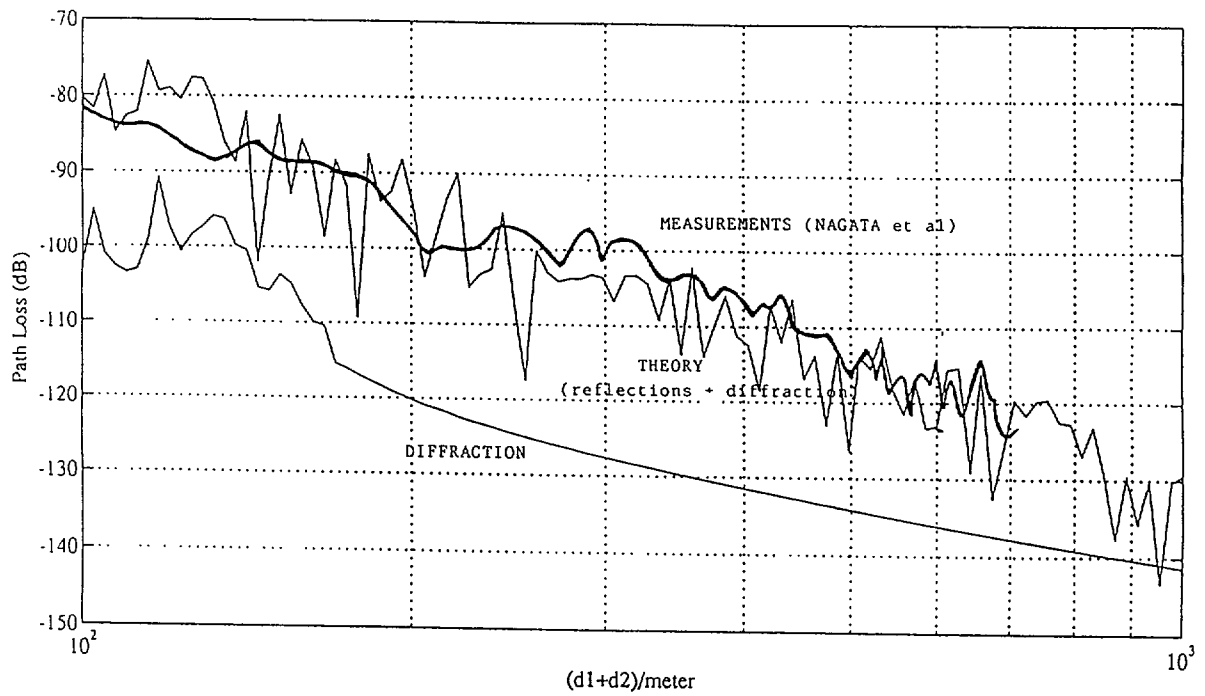


FIGURE 32: Comparison of predicted to measured signal levels for a side street receiver location. Shown here are the contributions of the diffracted fields to the total signal levels (from Yim et al. [17], page 205).

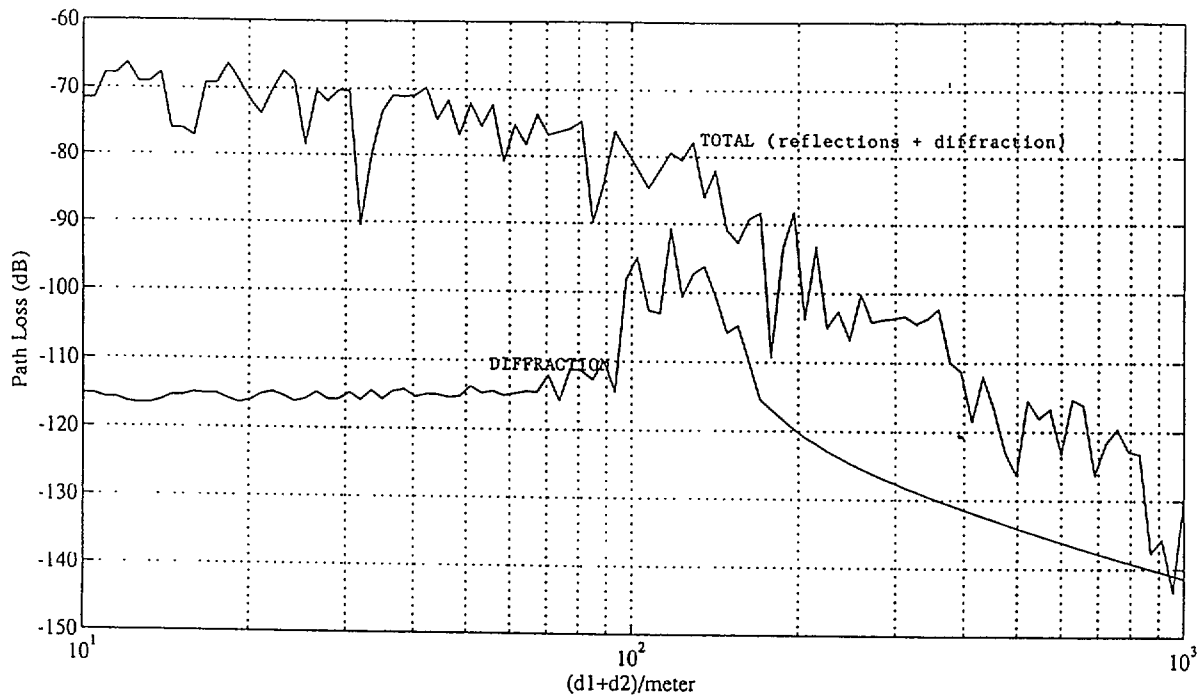


FIGURE 33: Signal levels for a side street receiver location. Show here are the contributions of the diffracted fields to the total signal levels (from Yim et al. [17], page 206).

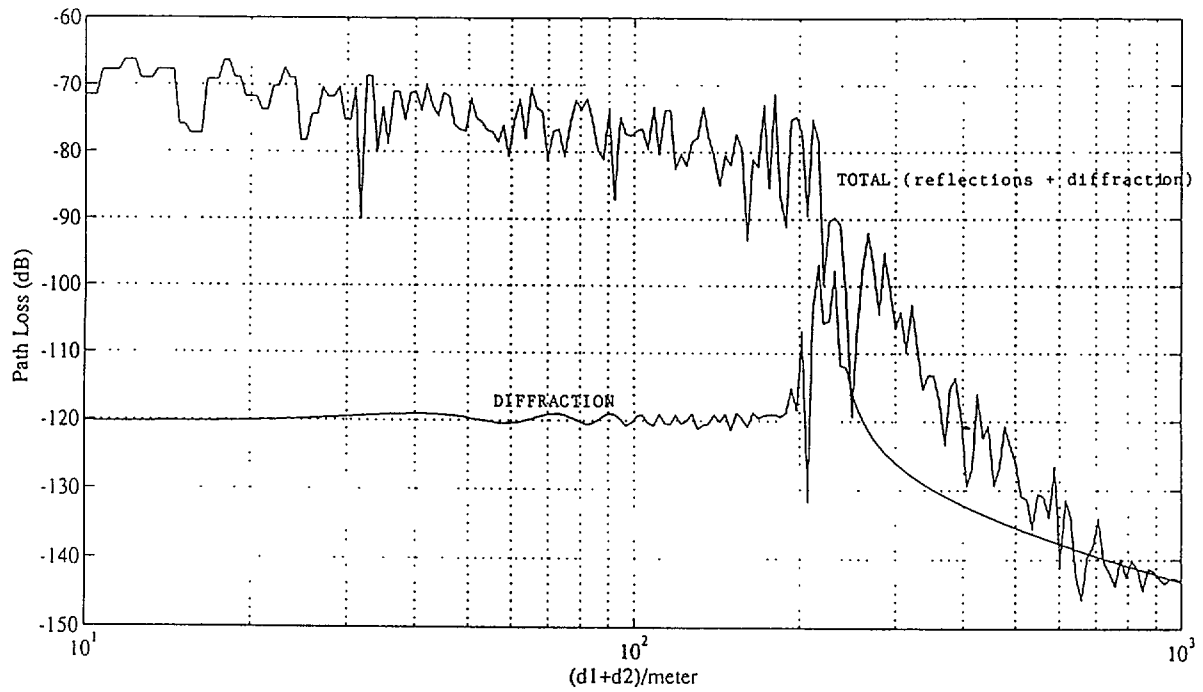


FIGURE 34: Signal levels for a side street receiver location. Show here are the contributions of the diffracted fields to the total signal levels (from Yim et al. [17], page 207).

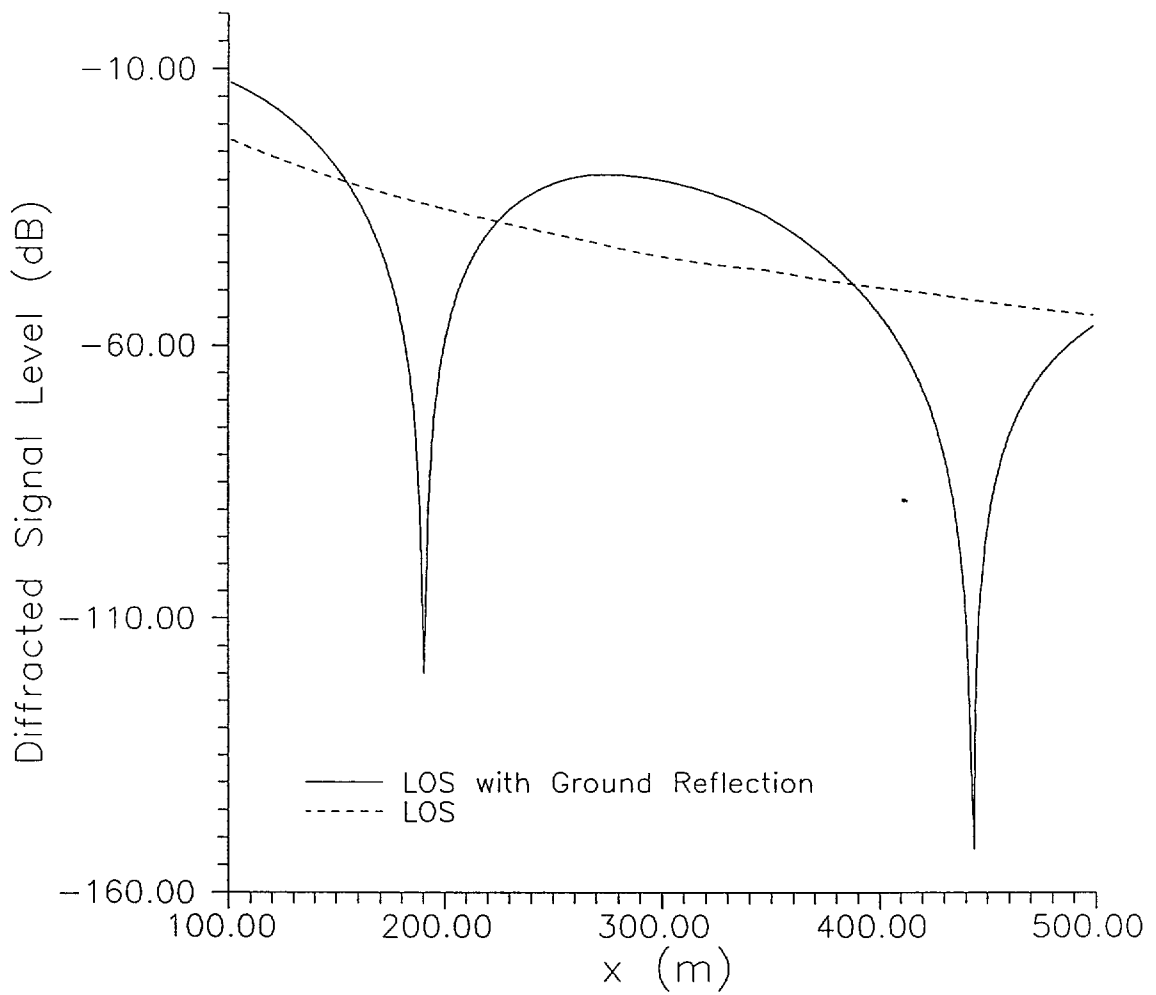


FIGURE 35: Comparison of the diffracted field signal levels obtained from just the LOS diffracted field and from the combination of both the LOS diffracted field and the ground reflected diffracted field. These results are for $f=10$ GHz, Tx height of 10m, and a Rx height of 10 m.

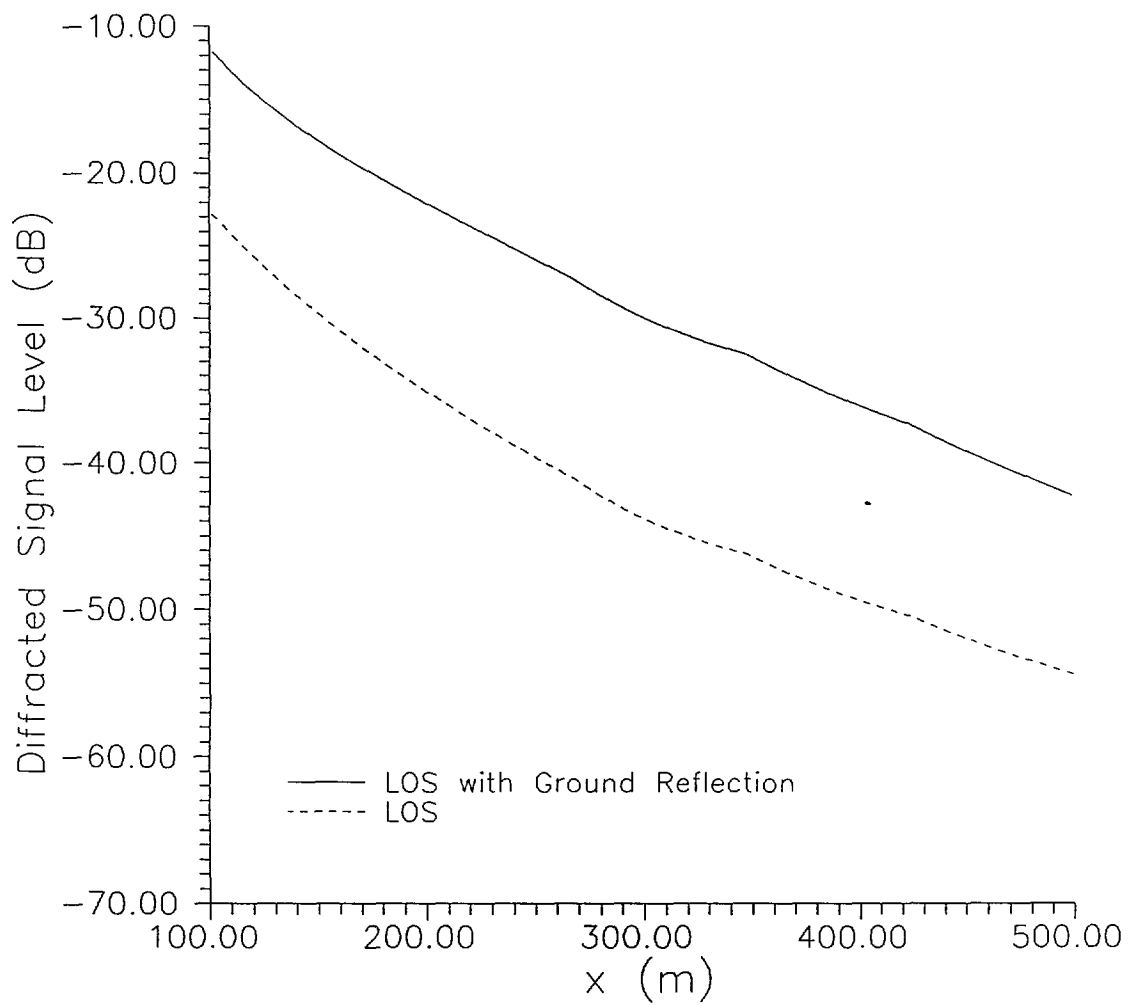


FIGURE 36: Comparison of the diffracted field signal levels obtained from just the LOS diffracted field and from the combination of both the LOS diffracted field and the ground reflected diffracted field. These results are for $f=10$ GHz, Tx height of 10m, and a Rx height of 2 m.

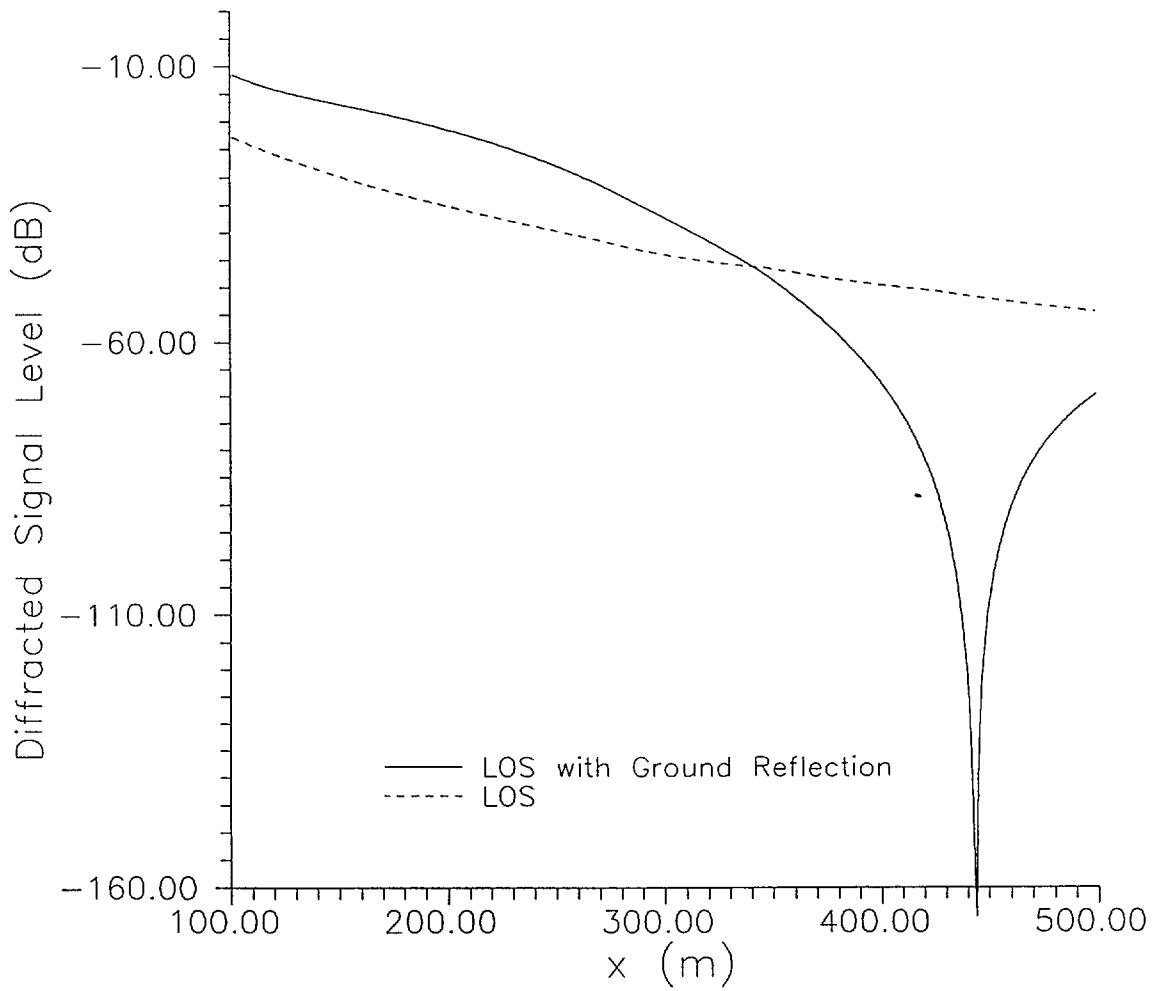


FIGURE 37: Comparison of the diffracted field signal levels obtained from just the LOS diffracted field and from the combination of both the LOS diffracted field and the ground reflected diffracted field. These results are for $f=5$ GHz, Tx height of 10m, and a Rx height of 10 m.

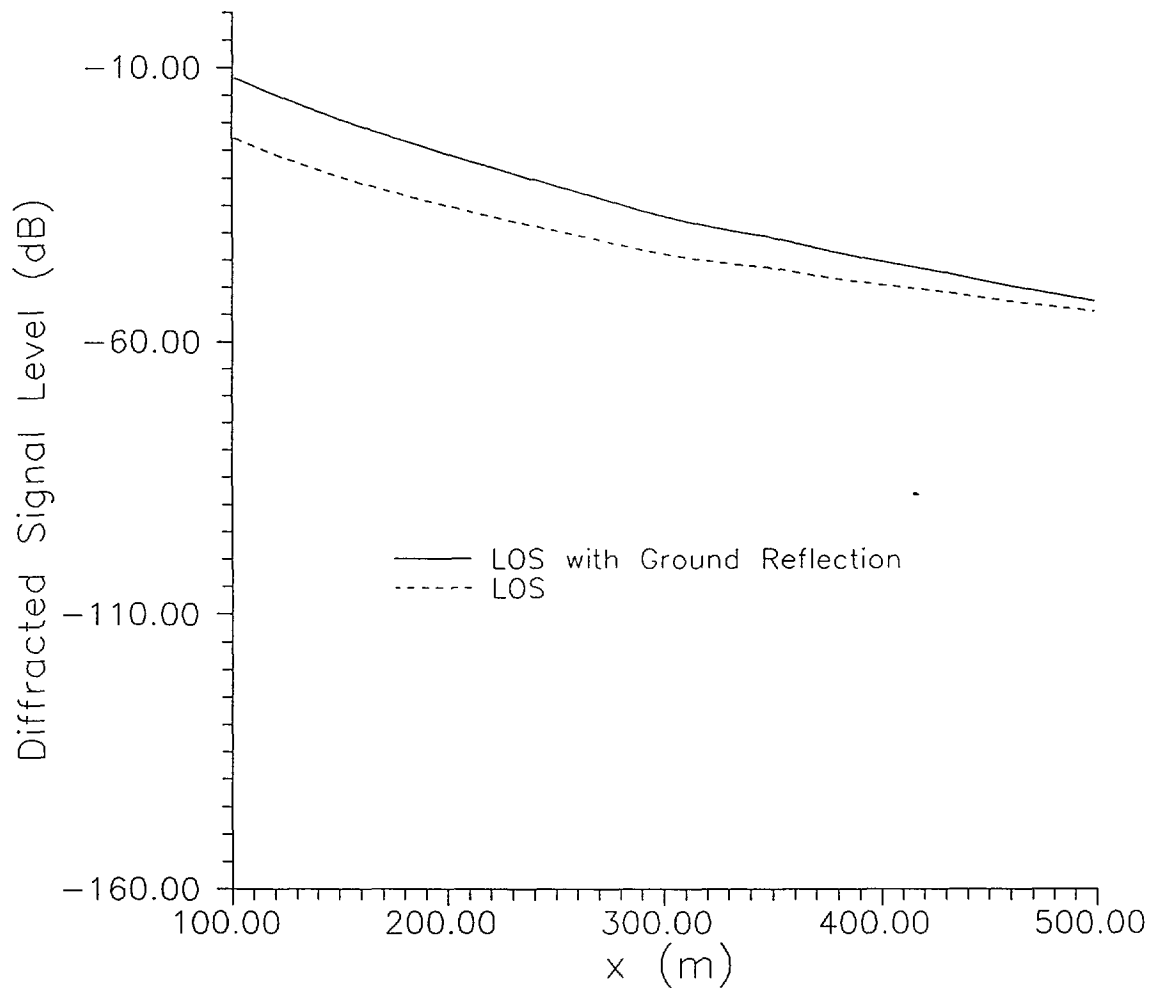


FIGURE 38: Comparison of the diffracted field signal levels obtained from just the LOS diffracted field and from the combination of both the LOS diffracted field and the ground reflected diffracted field. These results are for $f=5$ GHz, Tx height of 10m, and a Rx height of 2 m.

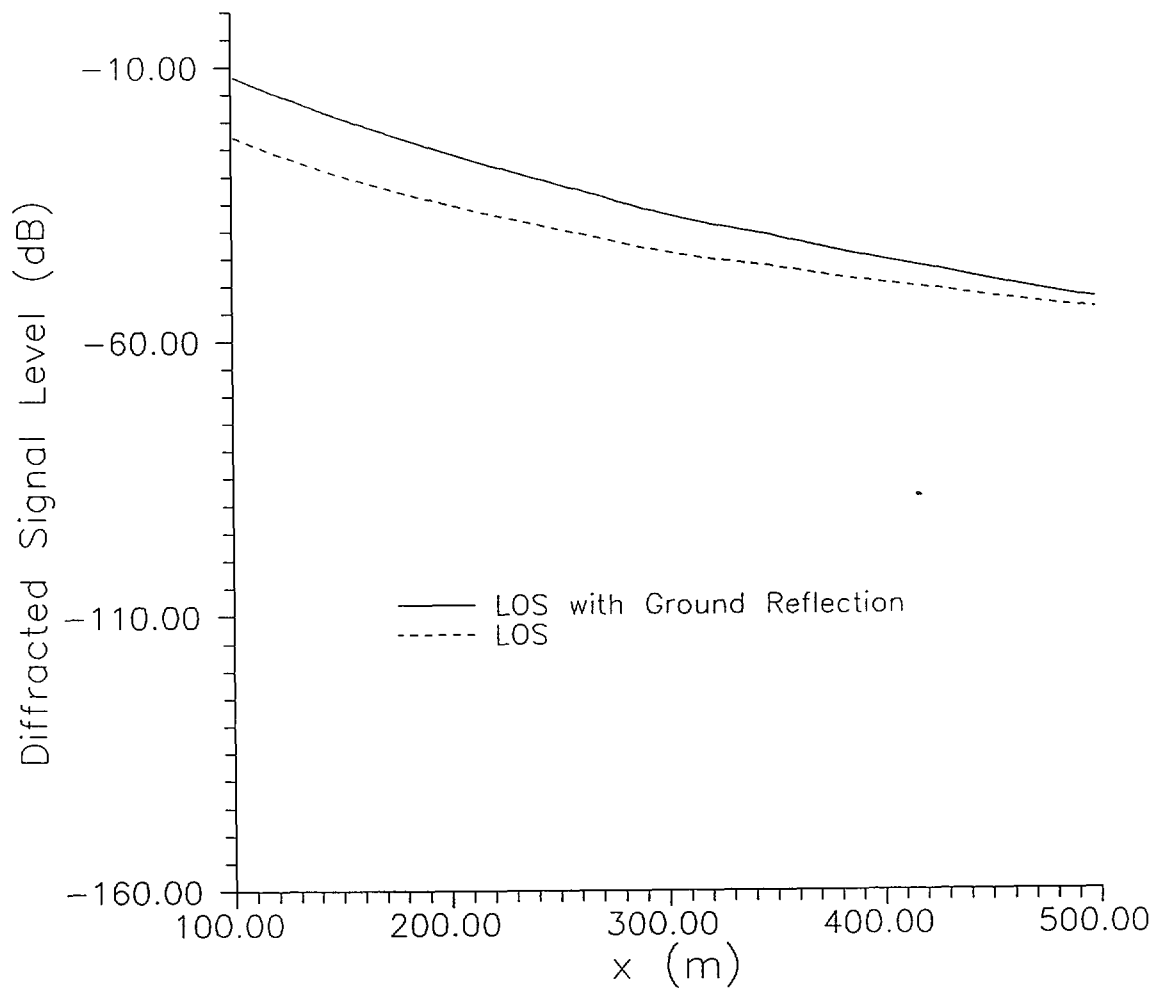


FIGURE 39: Comparison of the diffracted field signal levels obtained from just the LOS diffracted field and from the combination of both the LOS diffracted field and the ground reflected diffracted field. These results are for $f=1$ GHz, Tx height of 10m, and a Rx height of 10 m.

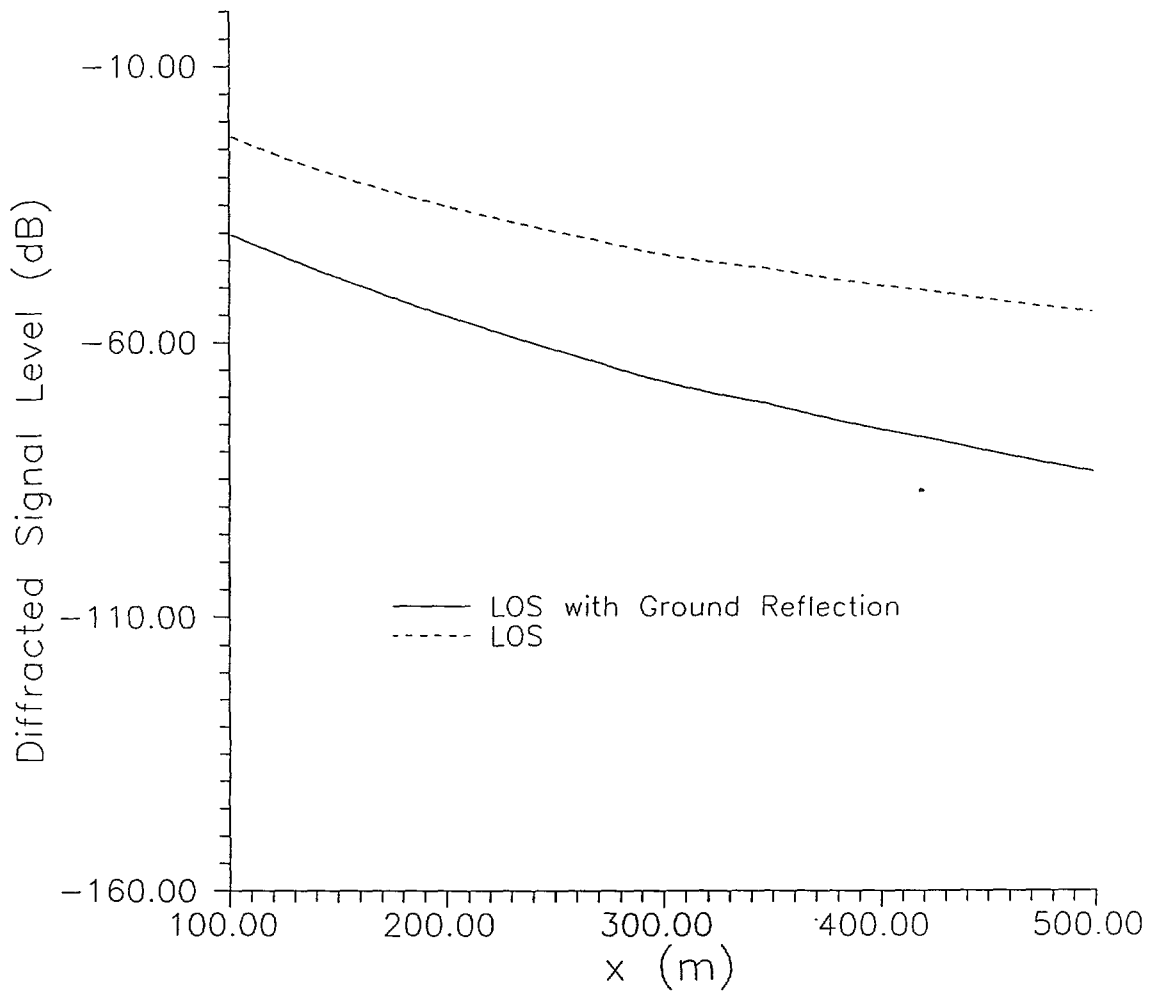


FIGURE 40: Comparison of the diffracted field signal levels obtained from just the LOS diffracted field and from the combination of both the LOS diffracted field and the ground reflected diffracted field. These results are for $f=1$ GHz, Tx height of 10m, and a Rx height of 2 m.

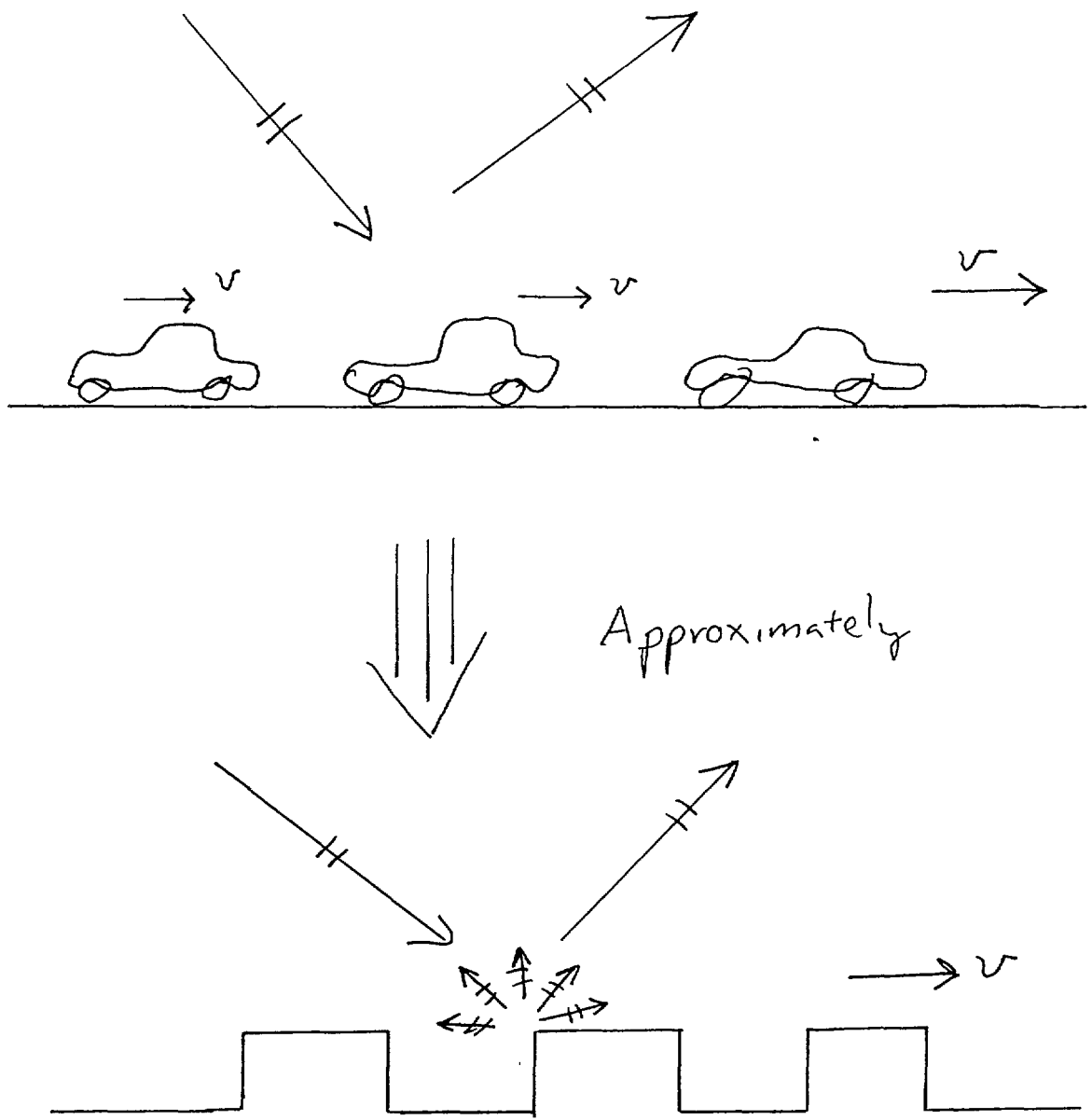


FIGURE 41: Illustration of a realistic street surface. Due to the automobiles, the street appears as a rough surface.

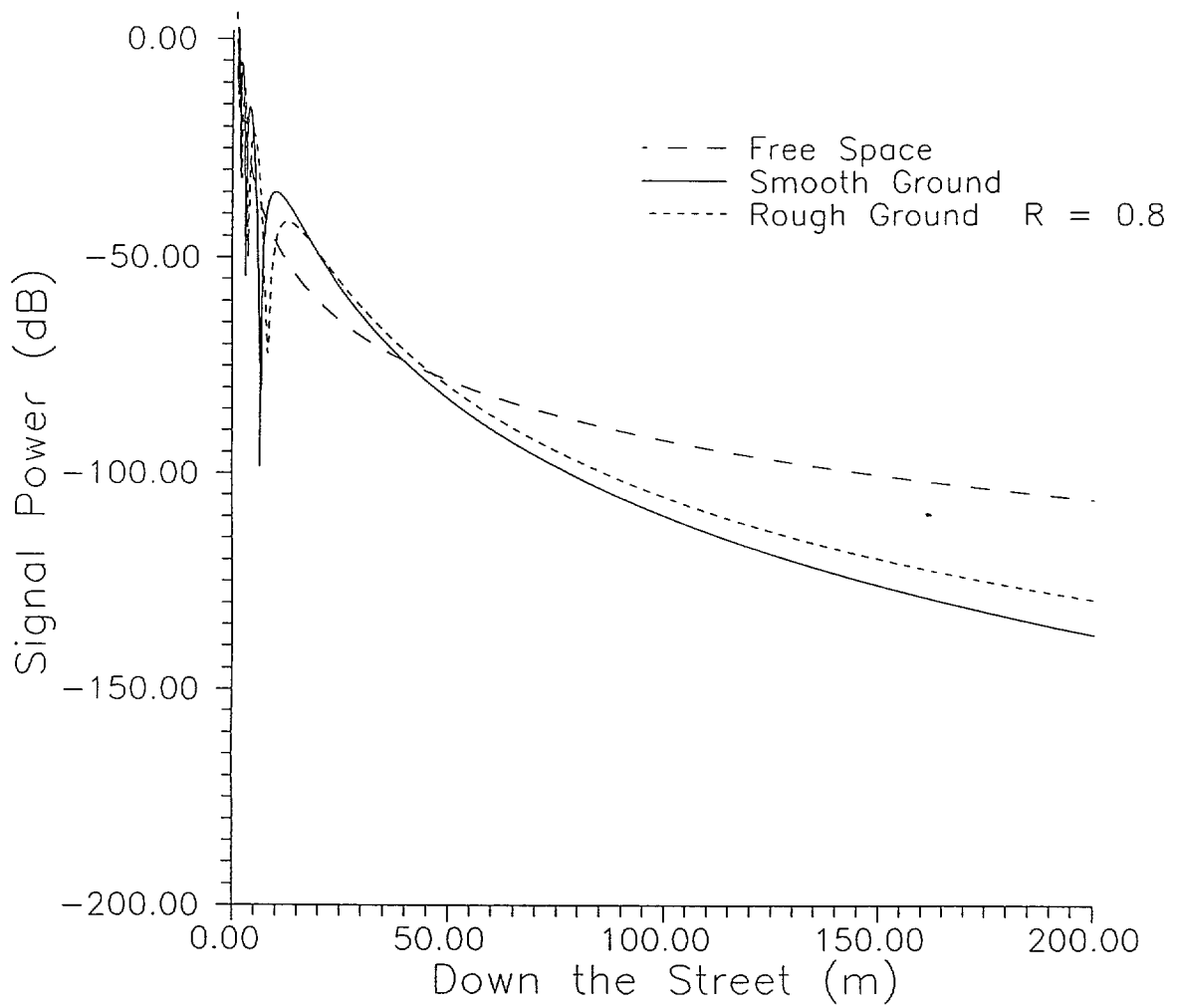


FIGURE 42: Illustration of the fading of a signal due to the LOS and ground reflection. These results are for a $f=1$ GHz and the Tx and Rx height equal to 1 m.

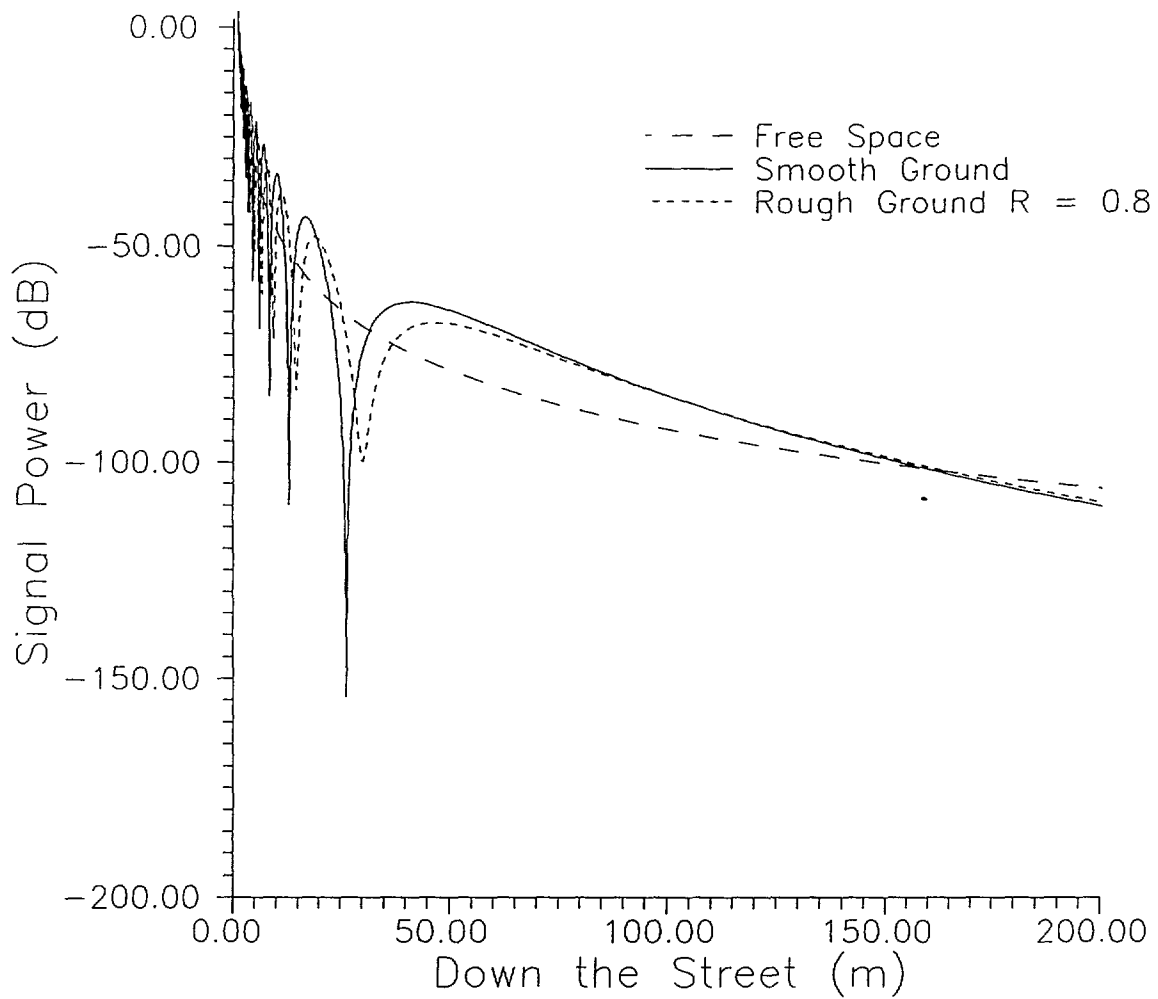


FIGURE 43: Illustration of the fading of a signal due to the LOS and ground reflection. These results are for a $f=1$ GHz and the Tx and Rx height equal to 2 m.

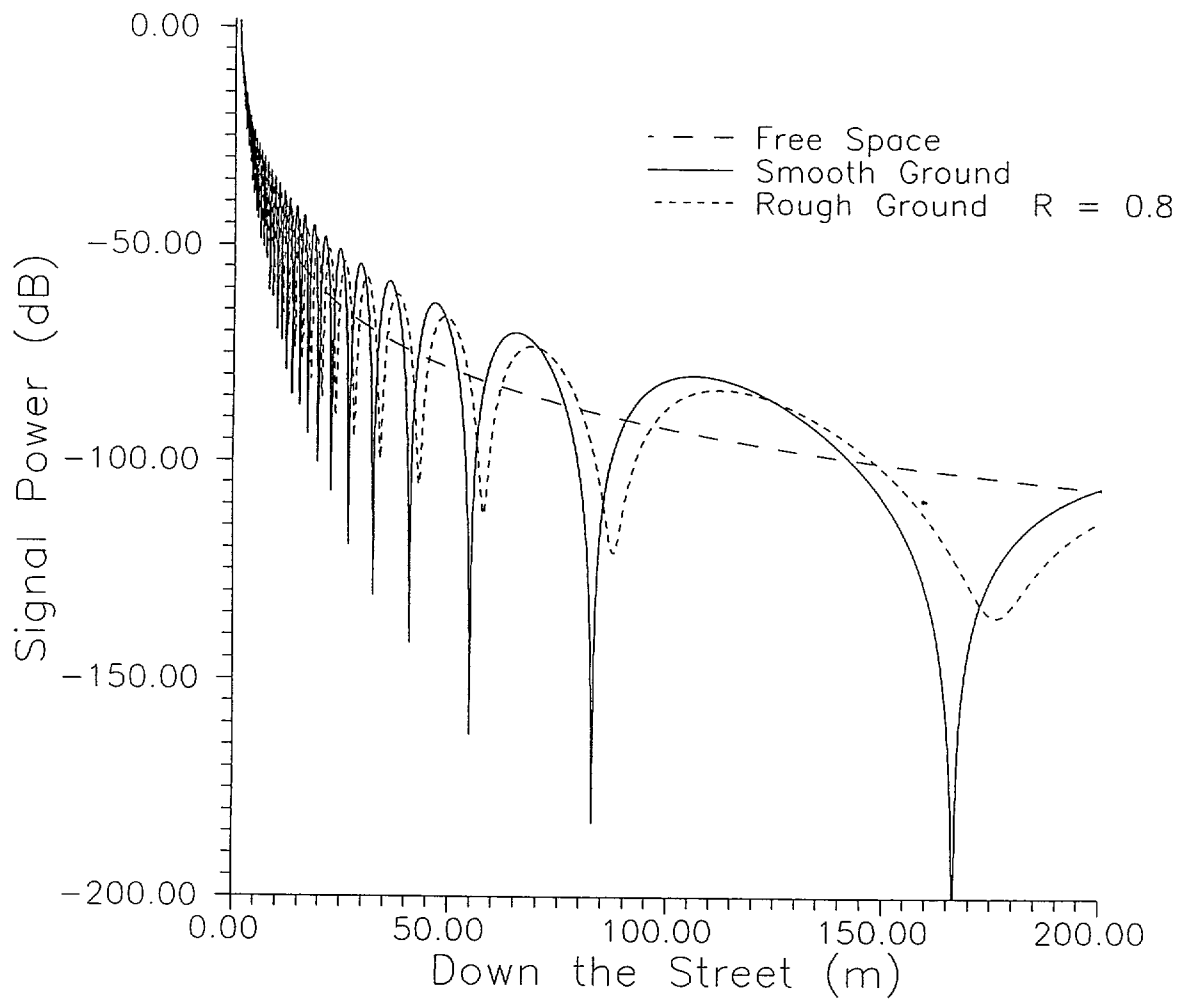


FIGURE 44: Illustration of the fading of a signal due to the LOS and ground reflection. These results are for a $f=1$ GHz and the Tx and Rx height equal to 5 m.

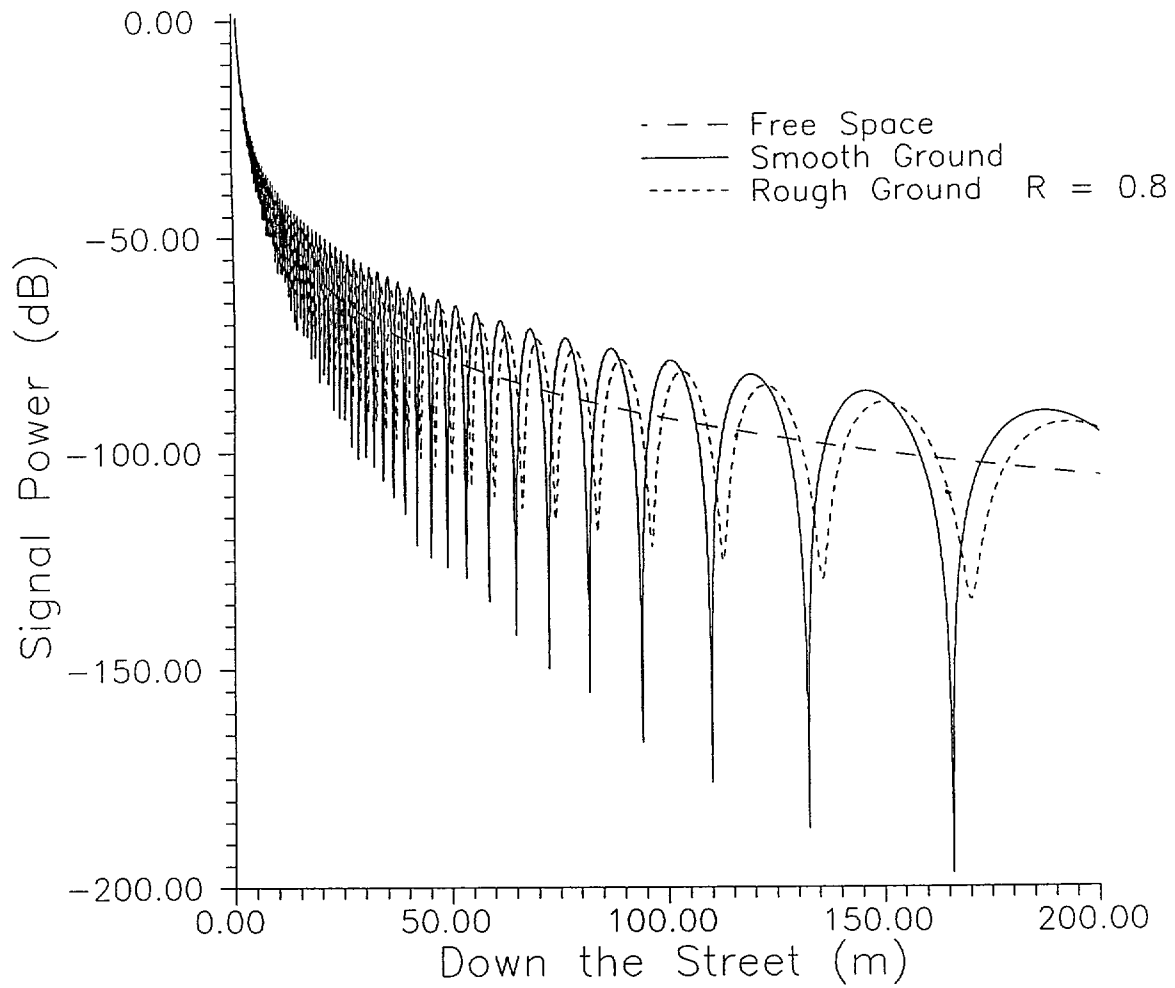


FIGURE 45: Illustration of the fading of a signal due to the LOS and ground reflection. These results are for a $f=1$ GHz and the Tx and Rx height equal to 10 m.

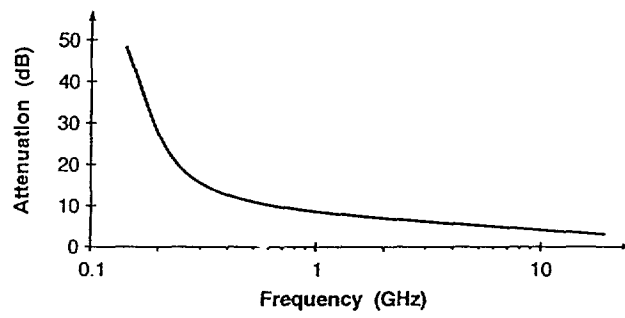


FIGURE 46: Attenuation in a tunnel for a LOS path (page 87 from Yacoub [54]).

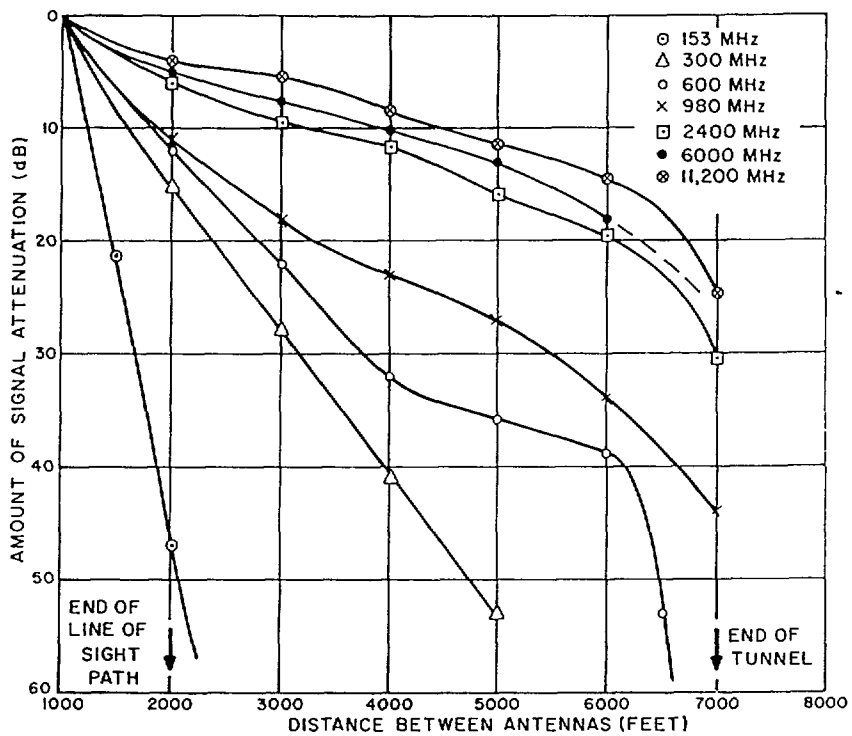


FIGURE 47: Attenuation in a tunnel for a LOS path (page 112 from Jakes [55]).

NTIA FORMAL PUBLICATION SERIES

NTIA MONOGRAPH

A scholarly, professionally oriented publication dealing with state-of-the-art research or an authoritative treatment of a broad area. A monograph is expected to have a long lifespan.

NTIA SPECIAL PUBLICATION

Information derived from or of value to NTIA activities such as conference proceedings, bibliographies, selected speeches, course and instructional materials, and directories.

NTIA HANDBOOK

Information pertaining to technical procedures: reference and data guides, and formal user's manuals that are expected to be pertinent for a long time.

NTIA REPORT

Important contributions to existing knowledge but of less breadth than a monograph, such as results of completed projects and major activities specific major accomplishments, or NTIA-coordinated activities.

NTIA RESTRICTED REPORT

Contributions that fit the Report classification but that are limited in distribution because of national security classification or Departmental constraints. This material receives full review and quality control equivalent to the open-literature report series.

NTIA CONTRACTOR REPORT

Information generated under an NTIA contract or grant and considered an important contribution to existing knowledge.

SPONSOR-ISSUED REPORTS

NTIA authors occasionally produce reports issued under an other-agency sponsor's cover. These reports generally embody the criteria of the NTIA Report series.

For information about NTIA publications, contact the Executive Office at 325 Broadway, Boulder, Colorado 80303 (telephone: 303-497-3572).
